Engineering Structures 195 (2019) 469–489

Contents lists available at ScienceDirect

Engineering Structures

journal homepage: www.elsevier.com/locate/engstruct

Optimal design for high-performance passive dynamic vibration absorbers under random vibration

Eduardo Barredo[a,*], J.G. Mendoza Larios[d], Jan Mayén[b], A.A. Flores-Hernández[a], Jorge Colín[a], M. Arias Montiel[c]

[a] Tecnológico Nacional de México/CENIDET, Interior Int. Palmira s/n, Col. Palmira, Cuernavaca, Morelos C.P. 62490, Mexico
[b] CIATEQ A. C., Eje 126 No. 225, Zona Industrial, San Luis Potosí, S.L.P. C.P. 78395, Mexico
[c] Universidad Tecnológica de la Mixteca, Instituto de Electrónica y Mecatrónica, C.P. 6900 Huajuapan de León, Oaxaca, Mexico
[d] Universidad Tecnológica de la Mixteca, Instituto de Ingeniería industrial y automotriz, C.P. 6900 Huajuapan de León, Oaxaca, Mexico

ARTICLE INFO

Keywords:
High-performance DVAs
Inerter
Optimization
Optimal design
Suppression band index

ABSTRACT

This work is motivated to determinate the optimal design for various types of Dynamic Vibration Absorbers (DVAs) under the effect of random loads. These devices are the following: DVAs connected in parallel or series; two degree-of-freedom traditional dynamic vibration absorber (2dof-TVA) with translational and rotational motion; and inerter-based DVAs (IDVA-C6, C4, and C3). These types of DVAs were selected by their high effectiveness for suppressing vibration however a comparative study on their dynamic performance has not yet been performed. Two different excitation sources of random loads are studied in this paper which are random ground motion and force excitation. An optimum design for majority of these devices has not yet been computed when subjected to random ground motion excitation, and therefore in this paper are computed. For random force excitation, some numerical solutions for the optimal design of these devices have not yet reported which in this paper are computed in order to compare the dynamic performance for each device with respect to that of the classic DVA. For both random excitation cases, the H_2 optimization criteria is used to analytically compute the variance of squared modulus of frequency response of the undamped primary structure, and then nonlinear unconstrained optimization problems are formulated in order to obtain the optimal design. Numerical solutions revealed that the IDVA-C6, C3, and DVAs connected in series presents more than 13% and 10% improvement with respect to the classic DVA for random ground motion and force excitation cases, respectively. These devices can widen the suppression band (SB) from 30% to 40% for mass ratios values from 1% to 10%. It means that devices are more effective and robust for mitigating vibration than the classic DVA. In addition, the rotational inertial double tuned mass damper (IDVA-C6) has the same relative dynamic performance (RDP) and suppression band index (SB) than the double-mass dynamic vibration absorber arranged in series. For practical application where the mounting space of the DVA is extremely reduced, the DVAs connected in series could be more convenient to use than IDVA-C6. The concept of equivalent mass ratio is introduced in order to explain the superiority of these devices with respect to the classic DVA. Finally, in H_∞ optimization criteria, the IDVA-C6 presents the same vibration amplitudes at all excitation frequency range and suppression band than DVAs connected in series.

1. Introduction

During the last decades, various types of mechanical devices have been proposed for the passive vibration control in civil engineering. These devices are known as the dynamic vibration absorbers (DVAs) or tuned mass dampers (TMDs) [1]. The main target of a DVA is to mitigate the dynamic response of mechanical structures under the effect of earthquakes, wind, maritime waves excitation, unbalanced rotating machinery, and dynamic vibration caused from vehicle traffic. In recent studies, the performance of the classic DVA has been enhanced by means of different connections of energy dissipation (dashpot) and absorption (spring) elements of the absorber, which the classic DVA is re-named as the non-traditional DVA, and Three-Element DVA [2–5]. In addition, different researches have been performed on the dynamic behavior of classic DVAs to improve the frequency response of the main structure when subjected to various types of excitation sources [6–10].

* Corresponding author.
E-mail address: eduardin_91@live.com.mx (E. Barredo).

https://doi.org/10.1016/j.engstruct.2019.05.105
Received 15 February 2019; Received in revised form 20 May 2019; Accepted 31 May 2019

Additionally, Krenk and Høgsberg introduced a classic DVA on a flexible structure to provide damping on a specific vibration mode, and thus reduce the dynamic magnification factor (DMF) of main structure [11]. They noted that the background flexibility of the main structure leads to higher design values for the absorber frequency and damping parameter. However, these improved DVAs only minimize the dynamic amplification factor of frequency response, but they do not improve the effective operating bandwidth or suppression band. In practice, various types of excitation sources of low and high frequency are presented, and the effective operating bandwidth or suppression band of the classic and improved DVAs is fixed which is the main disadvantage of these mechanical devices. For over this disadvantage, semi-active and active devices need to be implemented to the classic DVAs. In fact, Cheung et al. re-optimized the dynamic response for hybrid vibration absorber (HVA) which consists in an active damper for suppressing wide frequency band vibration [12]. Alujević et al. proposed inertial actuators (IAs) to yield active damping on a primary structure, and they noted that dynamic performance produced by IAs outperforms an optimally tuned classic TMD [13]. Gao et al. proposed adaptive DVAs to improve the dynamic performance for a vehicle power train system [14]. Recently, Shen et al. enhanced the operating bandwidth of the classic DVA by adding effects of negative dynamic stiffness in the system [15]. In addition, Xiuchang et al. provided optimal parameters for three kinds of isolation system with negative stiffness using the Routh–Hurwitz criterion and the stability boundary, and they noted that three-parameter isolator system outperforms dynamic performance of traditional DVA in controlling force transmission and mass response under harmonic and random vibration [16]. However, active energy dissipation elements need to be added for enhancing the performance of classic DVA which can be very expensive. Therefore, passive control by DVAs is yet effective in the vibration control, easy implementation, and low manufacturing cost.

Besides, dynamic characteristics for multiples DVAs arranged in parallel have been investigated in order to minimize the Dynamic Magnification Factor (DMF) and maximize the effective operating bandwidth of dynamic response of the primary structure [17–20]. In addition, different optimization algorithms have been proposed such as decentralized H_2 and H_∞ optimization, gradient method to improve the dynamic performance for multiples DVAs with uniformly distributed masses [21,22]. Those investigations revealed that there exist a specific number of DVAs for each mass ratio which yield the maximum performance in the system. In addition, Nan Li and Lei Ni demonstrated that the performance of multiples DVAs with non-uniformly distributed masses can be improved by adding some restrictions on the frequency spacing and damping of each DVA [23]. However, the applications for multiples DVAs arranged in parallel is limited to the mounting space yet. Some applications for these devices are the following; in machine tool structures for increasing the chatter resistance in machining process [24], periodic vibration suppressors in civil engineering [25]. Indeed, the DVAs arranged in parallel are more effective than classic DVAs for suppressing vibration, and the operating bandwidth is broadened.

Furthermore, the multiples DVA arranged in series are more effective and robustness than the multiples DVAs arranged in parallel and the Two degree-of-freedom Tuned Vibration Absorber (2dof TVA) [26–28]. The 2dof TVA exhibits two planar degrees of freedom, i.e. translational and rotational motion. In addition, the 2dof TVA has been applied to damp the dominant mode from the workpiece fixture, and the enhancement of machining stability [29]. In those investigations, it was noted that frequency response curves (FRFs) of the main structure both the DVAs arranged in parallel or series and the 2dof TVA are quite similar when optimized. In fact, by adding these mechanical devices the DMF of primary structure is drastically reduced, and the effective operating bandwidth is widened. Therefore, we can say that these devices present more effectiveness in suppressing vibration than traditional and improved DVAs.

Additionally, the inerter has shown to be another mechanical device of high-performance for the passive vibration control. This device was first proposed by Smith in order to enhance the dynamic behavior for a vehicle suspension system of Formula one cars [30–34]. Different alternatives of inerter designs have been proposed which are the following: the rack-and-pinion type inerter [35], ball-screw type inerter [36], continuously variable transmission (CVT) type inerter [37–39], and the hydraulic type inerter [40,41]. Further, the effectiveness of a classic DVA can be enhanced by adding an inerter in the system. In fact, Ikago et al. proposed the tuned viscous mass damper (TVMD) which consists in a spring connected in series with parallel arrangement of a dashpot and an inerter [42]. Chen et al. demonstrated that the inerter can modify the resonant frequencies in the system by means of the inertance constant, and thus tuns the external excitation frequencies [43]. Recently, Basili et al. proposed a novel structural configuration which consists in a mechanical network composed by one spring, one damper, and one inerter arranged in parallel, and they demonstrated that for nonconservative systems it is possible to obtain the connection parameters of spring-dashpot-inerter elements in order to minimize the most rapid decay of the time-domain structural response [44,45]. Marian and Giaralis proposed the tuned mass-damper–inerter (TMDI), and they noted that the TMDI is more effective than the classical TMD for a fixed value of the TMD mass in suppressing the displacement variance of white noise excited undamped SDOF primary structures [46]. Recently, Javidialesaadi and Wierschem proposed the Three-Element Vibration Absorber–Inerter (TEVAI), and they demonstrated that this device is able to provide a 3–10% and 3–14% reduction in the peak dynamic magnification factor, in comparison to the H_∞ and H_2 optimal TMDI, respectively [47]. Nevertheless, the TVMD, TMDI, and TEVAI can only reduce the vibration amplitudes, but they do not enlarge the effective operating bandwidth of the frequency response of the system. To address this issue different connections with spring, damper, and inerter have been proposed. These configurations are known as mechanical impedances or mechanical networks and have shown an improvement more than 10% with respect to that of the classic DVA. In fact, mechanical impedances C3, C4, and C6 showed to be the best for the passive vibration control. The proposed mechanical impedances were denominated as follows: the configuration C3 is a series connection of a spring, an inerter, and a damper; C6 is a spring in series to a parallel connection of an inerter and a damper; finally, an inerter in series to a parallel connection of a spring and a damper labeled as C4 [48,49]. Some of these impedances based on inerter have been applied for passive vibration control of beams [50], cables [51–53], seismic mitigation of storage tanks [54], vibration responses minimization for the wind turbine structures induced by wind and maritime waves [55,56], mitigation of the heave motion of offshore platforms [57], and structures interacting with the soil [58,59]. In addition, some researchers proposed the rotational inertial double tuned mass damper which results by replacing the damper of classic DVA by the mechanical impedance C6 [60–62]. According to these investigations, the dynamic behavior of inerter-based dynamic vibration absorbers (IDVAs) is quite like the DVAs arranged in parallel or series and the 2dof-TVA with translational and rotational motion. It was noted that, these mechanical devices can broaden the effective operating bandwidth of a classic DVA. In fact, the IDVAs, DVAs arranged in parallel or series, and 2dof TVA with translational and rotational motion use two vibration modes to damp the dominant mode of the primary structure. However, a comparative analysis on the dynamic performance of these devices have not yet been presented.

For the practice application of these devices in civil engineering, the installation in structures could be addressed as in previous investigations. For example, an experimental set-up for DVA arranged in series was conducted by Yasuda and Pan, and thus they presented experimental results for the case of harmonic force excitation [63,64]. On the other hand, the installation process for 2dof-TVA with translational and rotational motion can be seen in [29,65]. Experimental configurations

for IDVAs have not been yet reported however some mechanical realizations were reported in [31,34]. These mechanical realizations must be connected between the physical mass of the absorber and the primary structure. Although the excitation sources for the structures analyzed in those investigations are different to those of earthquakes or random ground excitation, the build and installation process of these devices can be performed as in previous researches. It is very important to mention that some nonlinearity (backlash, friction and elastic effects) of these devices can be deleted in the manufacturing process because they can deteriorate the dynamic performance.

According to the literature review, three types of high-performance passive dynamic vibration absorbers were noted which are the following; DVAs arranged in parallel or series, 2dof TVA with translational and rotational motion, and inerter-based dynamic vibration absorbers (IDVAs). These devices were selected by their high effectiveness in controlling vibration in fact they outperform the dynamic performance of improved and classic DVA. The underlying idea of this paper is to perform a comparative study on the dynamic performance of these devices under the effect of random and harmonic vibration in order to draw the advantages between them. For random vibration, two excitation cases are considered which are the following; random ground motion and force excitation on the primary structure of mass M_s. We select these excitation sources for the following concerns: first, optimum parameter values for design of DVAs arranged in parallel or series have not yet been provided considering the excitation sources proposed in this work [66,67]; second, for the 2dof-TVA with translational and rotational motion, random ground motion has not yet been considered for the dynamic behavior study of this device [26,29,68], and therefore the optimal parameters for this devices are computed here; third, for the IDVAs, random force excitation and harmonic force excitation were considered in previous studies [49,60,61,69], and for the random ground motion case, Javidialesaadi and Wierschem provided optimal solution for IDVA-C6 before. In this paper, the optimal numerical solutions for IDVA-C6 were taken with copyrights permission from [62] in order to compare the dynamic performance of these high-performance passive DVAs. For two random excitation cases, the H_2 optimization method is applied to minimize the variance of frequency responses of the main structure for each device. For harmonic vibration, the H_∞ optimization is considered in order to minimize the maximum vibration amplitudes at resonant frequencies of the system. Additionally, numerical simulations are performed for different values of mass ratio in order to calculate the improvement percentages for each device with respect to that of the classic DVA. In addition, the suppression band index is defined in order to compute the enlargement of effective operating range for each device. Finally, conclusions of this work are drawn.

2. Frequency response for high-performance DVAs

In this section, the calculations of frequency responses for the DVAs arranged in parallel or series, 2dof TVA with translational and rotational motion, and inerter-based dynamic vibration absorbers (IDVAs) are presented when subjected to random and harmonic vibration. Note that, some transfer functions for IDVAs have been derived before, which in this work were adapted with copyrights permission from [49,62,69]. In Fig. 2.1 three configurations of DVAs are depicted. The Fig. 2.1(a) represents a 2dof TVA with two degree-of-freedom (translation and rotation motion) which is composed by a solid bar of mass and rotational inertia m_1 and J_1, respectively. It may translate in the vertical direction and rotate around the mass center, as the primary structure, which is subjected to random ground motion and force excitation, is constrained to vibrate in the vertical direction only. The distances from the mass center to the set of springs and dampers of the 2dof TVA are given by d_1 and d_2. Zuo and Nayfeh showed that asymmetric connection ($d_1 \neq d_2$) of the locations of the connections between the 2dof TVA and primary structure provide more dynamic performance than symmetric connection ($d_1 = d_2 = d$) [26]. However, in practice, asymmetric connection is more difficult to implement than the another one. In fact, Yang et al. used a 2dof TVA configured in symmetric form for the milling vibration mitigation. They re-claimed that by setting radius ratio $a = \rho/d = \infty$, where ρ is the absorber's radius of gyration, the 2dof TVA design is equivalent to a classic DVA. If $a = 1$, the 2dof TVA design is equivalent to the DVA arranged in parallel showed in Fig. 2.1(c), which means that the mass m_1 of the 2dof TVA is equally distributed on two spring and damper location points [29]. Additionally, note that this device has two dampers (c_1 and c_2) and two springs (k_1 and k_2). The best performance of the 2dof TVA is also obtained when the damping coefficient c_2 takes negative values, which means an active damper need to be added to the absorber. Nevertheless, for the passive vibration control, negative damping cannot be achieved. Such a design could readily be implemented in an active absorber, though there would be potential for instabilities in the presence of modeling uncertainties [26]. Indeed, the presence of the second damper c_2 only influences the frequency response at high frequencies, well above the tuned frequencies of the 2dof TVA [68]. Therefore, for practice applications in passive structural vibration control, the 2fod TVA design must be done by properly choosing the radius ratio value a and setting the value of damper c_2 equal to zero.

On the other hand, in Fig. 2.1(b) and (c), the double-mass dynamic vibration absorbers arranged in parallel or series are depicted. Similarly, the best performance of double-mass DVAs arranged in series is obtained when damping constant c_1 takes negative values [70]. However, passive elements cannot yield negative damping. Therefore, the damping constant c_1 must be configured to be zero. For double-mass DVAs arranged in parallel, the damping coefficients c_1 and c_2 are

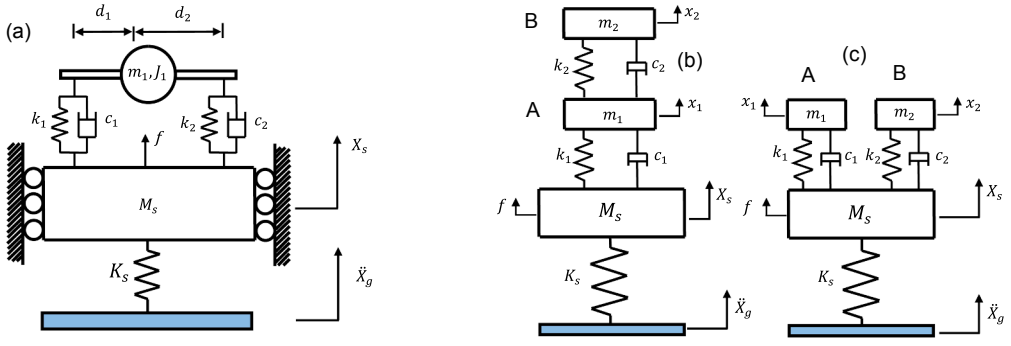

Fig. 2.1. Dynamic vibration absorbers (DVAs): (a) two degree-of-freedom dynamic vibration absorber with translational and rotational motion (2dof TVA); (b) DVAs arranged in series; (c) DVAs arranged in parallel.

positive [66,67].

Additionally, in this paper, the dynamic behavior of inerter-based dynamic vibration absorbers is analyzed under random ground motion, random force excitation, and harmonic vibration. The inerter is a mechanical device absorbs kinetic energy via a flywheel, then is released to yield a dynamic equilibrium among displacements of main structure mass M_s and the mass m_1. In addition, m_2 is the apparent mass o inertance constant of the inerter showed in Fig. 2.2. The IDVA can be obtained by replacing the damper of the classic DVA by some mechanical impedances C3, C4, and C6 showed in Fig. 2.2. Note that, Hu and Chen only derived optimal parameters for IDVAs under random force excitation [49], and optimal solutions of the IDVA-C6 have been provided for random ground motion excitation only [62]. It is important to mention that the main contribution of this article is the analysis and optimization for the mechanical devices showed in Fig. 2.1(a), (b), (c) and Fig. 2.2 under the effect of random ground motion, random force excitation, and harmonic force vibration.

Note that the devices depicted in Fig. 2.1(a), (b), (c) and Fig. 2.2 are three degree-of-freedom mechanical systems, except the IDVA-C3. The IDVA-C3 results by replacing the damper of classic DVA by the mechanical impedance C3 showed in Fig. 2.2, and therefore IDVA-C3 becomes a four degree-of-freedom system. The mathematical model for these devices can be written in general way by the following mathematical expression

$$\mathbf{M}\ddot{\boldsymbol{x}}(t) + \mathbf{C}\dot{\boldsymbol{x}}(t) + \mathbf{K}\boldsymbol{x}(t) = -\mathbf{M_g}\mathbf{I}\ddot{\boldsymbol{x}}_{\boldsymbol{g}}(t) + \mathbf{F}(t) \tag{2.1}$$

where $\mathbf{M}$, $\mathbf{C}$, $\mathbf{K}$ represent mass, damping, and stiffness matrices of the system, respectively. $\mathbf{M_g}$ denotes a mass diagonal matrix that contains the mass values, M_s, m_1 and m_2 for DVAs showed in Fig. 2.1(a), (b), (c), and $\mathbf{I}$ is an ones vector related to the external excitation $\ddot{\boldsymbol{x}}_{\boldsymbol{g}}(t)$. However, for the IDVAs showed in Fig. 2.2, the apparent mass m_2 is not present in the mass diagonal matrix $\mathbf{M_g}$, the values for the mass M_s and m_1 only. Indeed, the dynamic modelling for these devices under ground motion excitation is similar to that reported in [46]. Then, $\ddot{\boldsymbol{x}}_{\boldsymbol{g}}(t)$ and $\mathbf{F}(t)$ represent the base acceleration (e.g., seismic load) and external dynamic force excitation (e.g., wind load or unbalanced rotating machinery) in the system, and g is the acceleration due to gravity [59]. Considering that the system is subjected to harmonic ground acceleration and harmonic force excitation at frequency ω, represented as $\ddot{\boldsymbol{x}}_{\boldsymbol{g}}(t) = a_g e^{j\omega t}$ and $\mathbf{F}(t) = f_o e^{j\omega t}$. Then, the solution for the steady-state displacement vector $\boldsymbol{x}(\boldsymbol{\omega})$ in the frequency domain considering the base acceleration excitation $\ddot{\boldsymbol{x}}_{\boldsymbol{g}}(t)$ can be written as follows

$$\boldsymbol{x}(\boldsymbol{\omega}) = \mathbf{H}(\omega)(-\mathbf{M_g}\mathbf{I}\mathbf{A_g}) \tag{2.2}$$

Then, the response in steady-state $\boldsymbol{x}(\boldsymbol{\omega})$ when the system is subjected to the force excitation $\mathbf{F}(t)$ is as follows

$$\boldsymbol{x}(\boldsymbol{\omega}) = \mathbf{H}(\omega)(\mathbf{F}) \tag{2.3}$$

where $\mathbf{A_g}$ and $\mathbf{F}$ are matrices that contain the magnitudes a_g and f_o for excitation sources $\ddot{\boldsymbol{x}}_{\boldsymbol{g}}(t)$ and $\mathbf{F}(t)$, respectively. $\mathbf{H}(\omega)$ is the frequency response function matrix and is given by following mathematical expression

$$\mathbf{H}(\omega) = (-\omega^2\mathbf{M} + j\omega\mathbf{C} + \mathbf{K})^{-1} \tag{2.4}$$

It is convenient to select the following dimensionless variables to write in a dimensionless form the frequency responses $|H_{M_s}(\Omega)|$ for each device depicted in Fig. 2.1(a), (b), (c) and Fig. 2.2, which are the following

$$\beta = \frac{m_1}{M_s}, \quad \beta_1 = (1+\mu)\frac{m_1}{M_s}, \quad \mu = \frac{m_2}{m_1}, \quad \frac{1}{\sqrt{\alpha}} = \frac{\rho}{d}, \quad q = \frac{\omega_1}{\omega_s}, \quad \eta = \frac{\omega_2}{\omega_1}$$

$$\omega_s^2 = \frac{K_s}{M_s}, \quad \omega_1^2 = \frac{k_1}{m_1}, \quad \omega_2^2 = \frac{k_2}{m_2}, \quad \zeta_1 = \frac{c_1}{2\sqrt{k_1 m_1}}, \quad \zeta_2 = \frac{c_2}{2\sqrt{k_2 m_2}}, \quad \Omega = \frac{\omega}{\omega_s}$$

The definition for proposed dimensionless variables is as follows: first, for IDVAs, β is absorber-to-primary mass ratio, μ is apparent mass

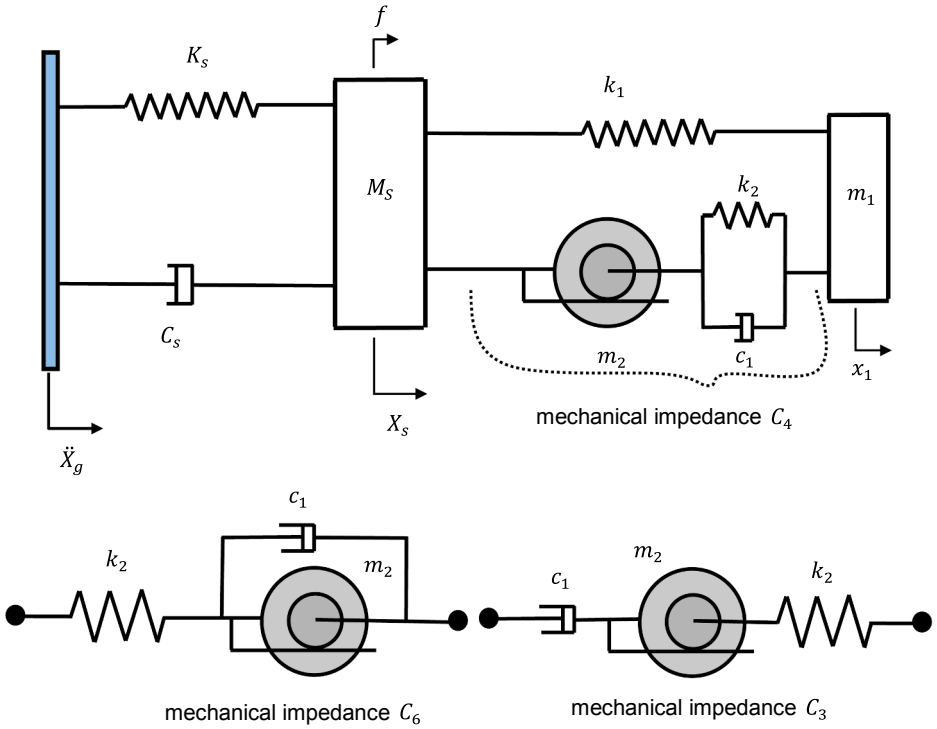

Fig. 2.2. Inerter-based dynamic vibration absorbers.

(inerter)-to-absorber mass ratio, q is natural frequency ratio, η is corner frequency ratio, ζ_1 is damping ratio for absorber of mass m_1, ω_s^2 is square natural frequency of the primary system, ω_1^2 is square natural frequency of the DVA, ω_2^2 is square corner frequency of the DVA; second, for the 2dof-TVA with translational and rotational motion, the name for β is conserved, $1/\sqrt{\alpha}$ is radius ratio, the name for q is conserved, η is re-named as the undamped natural frequency ratio of absorber with stiffness k_2 to the absorber with stiffness k_1 (see Fig. 2.1(a)), the name ζ_1 is conserved, then, for the name for ζ_2 is not available because the damper c_2 is configured to be equal zero, the name for ω_s^2 and ω_1^2 are similar as those of the IDVAs while ω_2^2 is natural frequency of absorber mass m_1 connected to stiffness k_2; and third, for DVAs arranged in parallel or series, β_1 is DVAs-to-primary mass ratio, μ is re-named as the DVA B to DVA A mass ratio, q and η are undamped natural frequencies ratio for DVA A and B, respectively. Then, ω_1^2 and ω_2^2 take the name of square natural frequency for DVA A and DVA B, respectively. Finally, Ω is the forced frequency ratio. Note that, the comparison of performance index between the IDVAs and DVAs arranged in series and parallel is possible because the physical mass of this device is small compared with the mass m_1 of the absorber. Really, this physical mass is the flywheel mass of the inerter and therefore the contribution to the translational kinetic energy into the system is small compared with that of physical mass m_1. On this fact, the dimensionless variables β_1 and β can be considered approximately equal or $\beta_1 \cong \beta$. Indeed, when the performance index of the IDVAs is compared with respect to that of classical DVA, the above assumption is applied [60].

According to the Eqs. (2.2) and (2.4), the frequency response functions $|H_{M_s}(\Omega)|$ of main structure for each device subject to base acceleration excitation $\ddot{\boldsymbol{x}}_{\boldsymbol{g}}(t)$, can be written as follow

$$
\begin{aligned}
|H_{DVAs-parallel}(\beta_1,\mu,q,\eta,\zeta_1,\zeta_2,\Omega)| &= \frac{X_s\omega_s^2}{a_g} = \left[\frac{A_1(\beta_1,\mu,q,\eta,\zeta_1,\zeta_2,\Omega)+B_1(\beta_1,\mu,q,\eta,\zeta_1,\zeta_2,\Omega)}{C_1(\beta_1,\mu,q,\eta,\zeta_1,\zeta_2,\Omega)+D_1(\beta_1,\mu,q,\eta,\zeta_1,\zeta_2,\Omega)}\right]^{\frac{1}{2}}\\
|H_{DVAs-series}(\beta_1,\mu,q,\eta,\zeta_2,\Omega)| &= \frac{X_s\omega_s^2}{a_g} = \left[\frac{A_2(\beta_1,\mu,q,\eta,\Omega)+B_2(\beta_1,\mu,q,\eta,\zeta_2,\Omega)}{C_2(\beta_1,\mu,q,\eta,\Omega)+D_2(\beta_1,\mu,q,\eta,\zeta_2,\Omega)}\right]^{\frac{1}{2}}\\
|H_{2dof-TVA}(\beta,\alpha,q,\eta,\zeta_1,\Omega)| &= \frac{X_s\omega_s^2}{a_g} = \left[\frac{A_3(\beta,\alpha,q,\eta,\Omega)+B_3(\beta,\alpha,q,\eta,\zeta_1,\Omega)}{C_3(\beta,\alpha,q,\eta,\Omega)+D_3(\beta,\alpha,q,\eta,\zeta_1,\Omega)}\right]^{\frac{1}{2}}\\
|H_{IDVA-C6}(\beta,\mu,q,\eta,\zeta_1,\Omega)| &= \frac{X_s\omega_s^2}{a_g} = \left[\frac{A_4(\beta,\mu,q,\eta,\Omega)+B_4(\beta,\mu,q,\eta,\zeta_1,\Omega)}{C_4(\beta,\mu,q,\eta,\Omega)+D_4(\beta,\mu,q,\eta,\zeta_1,\Omega)}\right]^{\frac{1}{2}}\\
|H_{IDVA-C4}(\beta,\mu,q,\eta,\zeta_1,\Omega)| &= \frac{X_s\omega_s^2}{a_g} = \left[\frac{A_5(\beta,\mu,q,\eta,\Omega)+B_5(\beta,\mu,q,\eta,\zeta_1,\Omega)}{C_5(\beta,\mu,q,\eta,\Omega)+D_5(\beta,\mu,q,\eta,\zeta_1,\Omega)}\right]^{\frac{1}{2}}\\
|H_{IDVA-C3}(\beta,\mu,q,\eta,\zeta_1,\Omega)| &= \frac{X_s\omega_s^2}{a_g} = \left[\frac{A_6(\beta,\mu,q,\eta,\zeta_1,\Omega)+B_6(\beta,\mu,q,\eta,\Omega)}{C_6(\beta,\mu,q,\eta,\zeta_1,\Omega)+D_6(\beta,\mu,q,\eta,\Omega)}\right]^{\frac{1}{2}}
\end{aligned}
\tag{2.5}
$$

In a similar way, the frequency responses $|H_{M_s}(\Omega)|$ of the main structure for each device under the effect of harmonic force excitation $\mathbf{F}(t)$ can be obtained using the equations (2.3) and (2.4), which are the following

$$
\begin{aligned}
|H_{DVAs-parallel}(\beta_1,\mu,q,\eta,\zeta_1,\zeta_2,\Omega)| &= \frac{X_sK_s}{f_0} = \left[\frac{A_{11}(\mu,q,\eta,\zeta_1,\zeta_2,\Omega)+B_{11}(\mu,q,\eta,\zeta_1,\zeta_2,\Omega)}{C_2(\beta_1,\mu,q,\eta,\zeta_1,\zeta_2,\Omega)+D_2(\beta_1,\mu,q,\eta,\zeta_1,\zeta_2,\Omega)}\right]^{\frac{1}{2}}\\
|H_{DVAs-series}(\beta_1,\mu,q,\eta,\zeta_2,\Omega)| &= \frac{X_sK_s}{f_0} = \left[\frac{A_{22}(\mu,q,\eta,\Omega)+B_{22}(\mu,q,\eta,\zeta_2,\Omega)}{C_1(\beta_1,\mu,q,\eta,\Omega)+D_1(\beta_1,\mu,q,\eta,\zeta_2,\Omega)}\right]^{\frac{1}{2}}\\
|H_{2dof-TVA}(\beta,\alpha,q,\eta,\zeta_1,\Omega)| &= \frac{X_sK_s}{f_o} = \left[\frac{A_{33}(\alpha,q,\eta,\Omega)+B_{33}(\alpha,q,\eta,\zeta_1,\Omega)}{C_3(\beta,\alpha,q,\eta,\Omega)+D_3(\beta,\alpha,q,\eta,\zeta_1,\Omega)}\right]^{\frac{1}{2}}\\
|H_{IDVA-C6}(\beta,\mu,q,\eta,\zeta_1,\Omega)| &= \frac{X_sK_s}{f_o} = \left[\frac{A_{44}(\mu,q,\eta,\Omega)+B_{44}(\mu,q,\eta,\zeta_1,\Omega)}{C_4(\beta,\mu,q,\eta,\Omega)+D_4(\beta,\mu,q,\eta,\zeta_1,\Omega)}\right]^{\frac{1}{2}}\\
|H_{IDVA-C4}(\beta,\mu,q,\eta,\zeta_1,\Omega)| &= \frac{X_sK_s}{f_o} = \left[\frac{A_{55}(\mu,q,\eta,\Omega)+B_{55}(\mu,q,\zeta_1,\Omega)}{C_5(\beta,\mu,q,\eta,\Omega)+D_5(\beta,\mu,q,\eta,\zeta_1,\Omega)}\right]^{\frac{1}{2}}\\
|H_{IDVA-C3}(\beta,\mu,q,\eta,\zeta_1,\Omega)| &= \frac{X_sK_s}{f_o} = \left[\frac{A_{66}(\mu,q,\eta,\zeta_1,\Omega)+B_{66}(\mu,q,\eta,\Omega)}{C_6(\beta,\mu,q,\eta,\zeta_1,\Omega)+D_6(\beta,\mu,q,\eta,\Omega)}\right]^{\frac{1}{2}}
\end{aligned}
\tag{2.6}
$$

The functions A_i, B_i, C_i, and D_i for $i = 1, \cdots, 6$ are described in Appendix A. In the next section, the optimization process is presented in order to compute the optimal design parameters for each device showed in Fig. 2.1(a), (b), (c) and Fig. 2.2 when subjected to random ground motion and force excitation. Subsequently, the performance for all devices is evaluated.

3. H_2 Optimization

3.1. Random ground motion and force excitation cases

For both excitation cases, we assume a stationary stochastic process represented in the frequency domain by a double-sided power spectral density (PSD) function $S(\omega) = S_0$ and with zero mean [71], as the excitation source on the base and mass M_s of primary structure. Note that, the response of a dynamic system subjected to a stationary random process is also a stationary random process [72]. Then, that dynamic response can be minimized by means of the H_2 optimization method. The performance measure in H_2 optimization can be written as [49]

$$
I = \frac{E[x^2]}{2\pi S_0\omega_n} \tag{3.1}
$$

where S_0 is the uniform power spectrum density function of the stationary process $S(\omega)$. The mean square value $E[x^2]$ of displacement of the main structure can be expressed as follows

$$
E[x^2] = S_0\int_{-\infty}^{+\infty}|H(j\omega)|^2d\omega = S_0\omega_n\int_{-\infty}^{+\infty}|H(j\Omega)|^2d\Omega \tag{3.2}
$$

where $H(j\Omega)$ is the frequency response of the main structure mass M_s for each device showed in Fig. 2.1(a), (b), (c) and Fig. 2.2. Substituting the Eq. (3.2) into (3.1), it yields

$$
I = \frac{1}{2\pi}\int_{-\infty}^{+\infty}|H(j\Omega)|^2d\Omega \tag{3.3}
$$

Note that the Eq. (3.3) is the variance σ_i^2 of frequency response $|H(j\Omega)|^2$ of the main structure [71]. Therefore, the variances for each device under the effect for both random ground motion and force excitation can be calculated in a general form as follow

$$
\begin{aligned}
\sigma^2_{DVAs-Parallel}(\beta_1,\mu,q,\eta,\zeta_1,\zeta_2) &= \frac{1}{2\pi}\int_{-\infty}^{+\infty}|H_{DVAs-parallel}(\beta_1,\mu,q,\eta,\zeta_1,\zeta_2,\Omega)|^2d\Omega\\
\sigma^2_{DVAs-series}(\beta_1,\mu,q,\eta,\zeta_2) &= \frac{1}{2\pi}\int_{-\infty}^{+\infty}|H_{DVAs-series}(\beta_1,\mu,q,\eta,\zeta_2,\Omega)|^2d\Omega\\
\sigma^2_{2dof-TVA}(\beta,\alpha,q,\eta,\zeta_1) &= \frac{1}{2\pi}\int_{-\infty}^{+\infty}|H_{2dof-TVA}(\beta,\alpha,q,\eta,\zeta_1,\Omega)|^2d\Omega\\
\sigma^2_{IDVA-C6}(\beta,\mu,q,\eta,\zeta_1) &= \frac{1}{2\pi}\int_{-\infty}^{+\infty}|H_{IDVA-C6}(\beta,\mu,q,\eta,\zeta_1,\Omega)|^2d\Omega\\
\sigma^2_{IDVA-C4}(\beta,\mu,q,\eta,\zeta_1) &= \frac{1}{2\pi}\int_{-\infty}^{+\infty}|H_{IDVA-C4}(\beta,\mu,q,\eta,\zeta_1,\Omega)|^2d\Omega\\
\sigma^2_{IDVA-C3}(\beta,\mu,q,\eta,\zeta_1) &= \frac{1}{2\pi}\int_{-\infty}^{+\infty}|H_{IDVA-C3}(\beta,\mu,q,\eta,\zeta_1,\Omega)|^2d\Omega
\end{aligned}
\tag{3.4}
$$

Note that the integrals given by the Eq. (3.4) are improper integrals and can be solved by residue integration method [73]. In addition, note that the expression mathematical $\frac{1}{2\pi}\int_{-\infty}^{+\infty}|H(j\Omega)|^2d\Omega$ is the standard $\|H(s)\|_2^2 = \|C(sI-A)^{-1}B\|_2^2 = \mathrm{Trace}(CLC^{\mathrm{T}})$ norm and can be computed from a minimal state-space realization $H(s)$, which consist in to analytically solve the Lyapunov equation [32]. During the calculation for these integrals, we observed that the denominator of the primary structure frequency response for each device showed in Fig. 2.1(a), (b), (c) and Fig. 2.2 has six simple poles in the upper half of the complex plane. Indeed, Asami found that the denominator of frequency response of the DVAs arranged in parallel or series also has six simple poles, and therefore the improper integrals can be calculated by means of the sum of the six residues yielded at each simple pole or by means of following mathematical expression $\int_{-\infty}^{+\infty}f_n(\lambda)\mathrm{d}\lambda = 2\pi i\sum_{k=1}^{6}\mathrm{Res}[f_n; i\lambda_k]$ [70]. By using the Asami's approach, an analytical solution can be found for each integral given by Eq. (3.4). First, for the random ground motion excitation case, the set of equations (2.5) must be substituted into (3.4), then an analytical solution for the variance of the frequency response of the primary structure for each device can be obtained as follows

$$\sigma^2_{DVAs-Parallel}(\beta_1,\mu,q,\eta,\zeta_1,\zeta_2) = \frac{\begin{array}{l} f_1(\beta_1,\mu,q,\zeta_1,\zeta_2)\eta^8 + f_2(\beta_1,\mu,q,\zeta_1,\zeta_2)\eta^7 + f_3(\beta_1,\mu,q,\zeta_1,\zeta_2)\eta^6 + f_4(\beta_1,\mu,q,\zeta_1,\zeta_2)\eta^5 \\ + f_5(\beta_1,\mu,q,\zeta_1,\zeta_2)\eta^4 + f_6(\beta_1,\mu,q,\zeta_1,\zeta_2)\eta^3 + f_7(\beta_1,\mu,q,\zeta_1,\zeta_2)\eta^2 + f_8(\beta_1,\mu,q,\zeta_1,\zeta_2)\eta \\ + f_9(\beta_1,\mu,q,\zeta_1,\zeta_2) \end{array}}{\begin{array}{l} g_1(\beta_1,\mu,q,\zeta_1,\zeta_2)\eta^8 + g_2(\beta_1,\mu,q,\zeta_1,\zeta_2)\eta^7 + g_3(\beta_1,\mu,q,\zeta_1,\zeta_2)\eta^6 + g_4(\beta_1,\mu,q,\zeta_1,\zeta_2)\eta^5 \\ + g_5(\beta_1,\mu,q,\zeta_1,\zeta_2)\eta^4 + g_6(\beta_1,\mu,q,\zeta_1,\zeta_2)\eta^3 + g_7(\beta_1,\mu,q,\zeta_1,\zeta_2)\eta^2 + g_8(\beta_1,\mu,q,\zeta_1,\zeta_2)\eta \\ + g_9(\beta_1,\mu,q,\zeta_1,\zeta_2) \end{array}}$$

$$\sigma^2_{DVAs-series}(\beta_1,\mu,q,\eta,\zeta_2) = \frac{f_{10}(\beta_1,\mu,q,\zeta_2)\eta^4 + f_{11}(\beta_1,\mu,q,\zeta_2)\eta^2 + f_{12}(\beta_1,\mu,q,\zeta_2)}{4(1+\mu)q^5\zeta_2\eta\mu\beta_1}$$

$$\sigma^2_{2dof-TVA}(\beta,\alpha,q,\eta,\zeta_1) = \frac{f_{13}(\beta,\alpha,q,\zeta_1)\eta^6 + f_{14}(\beta,\alpha,q,\zeta_1)\eta^4 + f_{15}(\beta,\alpha,q,\zeta_1)\eta^2 + f_{16}(\beta,\alpha,q)}{4q\beta\zeta_1\eta^2(1+2\alpha^2q^2\eta^2 - (1+2q^2(1+\beta_1)\eta^2)\alpha)^2}$$

$$\sigma^2_{IDVA-C6}(\beta,\mu,q,\eta,\zeta_1) = \frac{f_{17}(\beta,\mu,q,\zeta_1)\eta^4 + f_{18}(\beta,\mu,q,\zeta_1)\eta^2 + f_{19}(\beta,\mu,q,\zeta_1)}{4\zeta_1q^5\eta^4\mu^2\beta}$$

$$\sigma^2_{IDVA-C4}(\beta,\mu,q,\eta,\zeta_1) = \frac{f_{20}(\beta,\mu,q,\zeta_1)\eta^4 + f_{21}(\beta,\mu,q,\zeta_1)\eta^2 + f_{22}(\beta,\mu,q,\zeta_1)}{4q\zeta_1\beta\mu^2}$$

$$\sigma^2_{IDVA-C3}(\beta,\mu,q,\eta,\zeta_1) = \frac{f_{23}(\beta,\mu,q,\zeta_1)\eta^4 + f_{24}(\beta,\mu,q,\zeta_1)\eta^2 + f_{25}(\beta,\mu,q,\zeta_1)}{4\eta^4\mu^2q^3\zeta_1\beta} \tag{3.5}$$

Then, for random force excitation case, the set equations given by Eq. (2.6) must be used to calculate the variance for each device, is that, the magnitudes $|H_{DVAs-parallel}(\beta_1,\mu,q,\eta,\zeta_1,\zeta_2,\Omega)|$, $|H_{DVAs-series}(\beta_1,\mu,q,\eta,\zeta_2,\Omega)|$, $|H_{2dof-TVA}(\beta,\alpha,q,\eta,\zeta_1,\Omega)|$, $|H_{IDVA-C6}(\beta,\mu,q,\eta,\zeta_1,\Omega)|$, $|H_{IDVA-C4}(\beta,\mu,q,\eta,\zeta_1,\Omega)|$, and $|H_{IDVA-C3}(\beta,\mu,q,\eta,\zeta_1,\Omega)|$ must be substituted into Eq. (3.4). Then, the formulation for the analytical solution of resulting improper integrals is quite similar to the random ground motion excitation case. Therefore, it results in

$$\sigma^2_{DVAs-Parallel}(\beta_1,\mu,q,\eta,\zeta_1,\zeta_2) = \frac{\begin{array}{l} F_1(\beta_1,\mu,q,\zeta_1,\zeta_2)\eta^8 + F_2(\beta_1,\mu,q,\zeta_1,\zeta_2)\eta^7 + F_3(\beta_1,\mu,q,\zeta_1,\zeta_2)\eta^6 \\ + F_4(\beta_1,\mu,q,\zeta_1,\zeta_2)\eta^5 + F_5(\beta_1,\mu,q,\zeta_1,\zeta_2)\eta^4 + F_6(\beta_1,\mu,q,\zeta_1,\zeta_2)\eta^3 \\ + F_7(\beta_1,\mu,q,\zeta_1,\zeta_2)\eta^2 + F_8(\beta_1,\mu,q,\zeta_1,\zeta_2)\eta + F_9(\beta_1,\mu,q,\zeta_1,\zeta_2) \end{array}}{\begin{array}{l} G_1(\beta_1,\mu,q,\zeta_1,\zeta_2)\eta^8 + G_2(\beta_1,\mu,q,\zeta_1,\zeta_2)\eta^7 + G_3(\beta_1,\mu,q,\zeta_1,\zeta_2)\eta^6 \\ + G_4(\beta_1,\mu,q,\zeta_1,\zeta_2)\eta^5 + G_5(\beta_1,\mu,q,\zeta_1,\zeta_2)\eta^4 + G_6(\beta_1,\mu,q,\zeta_1,\zeta_2)\eta^3 \\ + G_7(\beta_1,\mu,q,\zeta_1,\zeta_2)\eta^2 + G_8(\beta_1,\mu,q,\zeta_1,\zeta_2)\eta + G_9(\beta_1,\mu,q,\zeta_1,\zeta_2) \end{array}}$$

$$\sigma^2_{DVAs-series}(\beta_1,\mu,q,\eta,\zeta_2) = \frac{F_{10}(\beta_1,\mu,q,\zeta_2)\eta^4 + F_{11}(\beta_1,\mu,q,\zeta_2)\eta^2 + F_{12}(\beta_1,\mu,q,\zeta_2)}{4q^5\zeta_2\eta\mu\beta_1}$$

$$\sigma^2_{2dof-TVA}(\beta,\alpha,q,\eta,\zeta_1) = \frac{F_{13}(\beta,\alpha,q,\zeta_1)\eta^4 + F_{14}(\beta,\alpha,q,\zeta_1)\eta^2 + F_{15}(\alpha,\beta,q,\zeta_1)}{16q\beta\zeta_1(\alpha q^2(\beta_1-\alpha+1)\eta^2 + 0.5\alpha - 0.5)^2}$$

$$\sigma^2_{IDVA-C6}(\beta,\mu,q,\eta,\zeta_1) = \frac{F_{16}(\beta,\mu,q,\zeta_1)\eta^4 + F_{17}(\beta,\mu,q,\zeta_1)\eta^2 + F_{18}(\beta,\mu,q,\zeta_1)}{4\zeta_1q^5\eta^4\mu^2\beta}$$

$$\sigma^2_{IDVA-C4}(\beta,\mu,q,\eta,\zeta_1) = \frac{F_{19}(\beta,\mu,q,\zeta_1)\eta^4 + F_{20}(\beta,\mu,q,\zeta_1)\eta^2 + F_{21}(\beta,\mu,q,\zeta_1)}{4q\zeta_1\beta\mu^2}$$

$$\sigma^2_{IDVA-C3}(\beta,\mu,q,\eta,\zeta_1) = \frac{F_{22}(\beta,\mu,q,\zeta_1)\eta^4 + F_{23}(\beta,\mu,q,\zeta_1)\eta^2 + F_{24}(\beta,q,\zeta_1)}{4\eta^4\mu^2q^3\zeta_1\beta} \tag{3.6}$$

where F_i and G_j for $i = 1, \cdots, 24$ and $j = 1, \cdots, 9$ and f_i and g_j for $i = 1, \cdots, 25$ and $j = 1, \cdots, 9$ are functions in terms of dimensionless variables $\beta, \beta_1, \mu, \alpha, q, \zeta_1, \zeta_2$. These dimensionless functions are depicted in Appendix C.

For both random vibration excitation cases, in a general way, optimal solution for the H_2 norm can be obtained by forcing each equation (analytical variance) from set of Eqs. (3.5) and (3.6) to the following conditions $\partial\sigma^2_{DVAs-types}/\partial\mu = 0$, $\partial\sigma^2_{DVAs-types}/\partial\alpha = 0$, $\partial\sigma^2_{DVAs-types}/\partial q = 0$, $\partial\sigma^2_{DVAs-types}/\partial\eta = 0$, $\partial\sigma^2_{DVAs-types}/\partial\zeta_1 = 0$, and $\partial\sigma^2_{DVAs-types}/\partial\zeta_2 = 0$. The subscript DVAs-types denotes to the DVAs types, is that, the DVAs arranged in parallel or series, 2dof TVA with translational and rotational motion, and inerter-based DVAs. These conditions yield simultaneous equations which can be numerically solved by Newton–Raphson method [70]. Then, for a constant mass ratio β or β_1, the optimal solutions for μ_{opt}, α_{opt}, q_{opt}, η_{opt}, $\zeta_{1,opt}$, and $\zeta_{2,opt}$ can be computed by solving those conditions. An alternative approach to calculate optimal parameters that minimize the variances of squared modulus of the FRF $|H(j\Omega)|^2$ of the primary structure is to use *Global Optimization Toolbox* provided by the software Maplesoft [74]. Therefore, in this paper, Maplesoft optimization toolbox is used for the minimization of each variance given by the set of Eqs. (3.5) and (3.6), and the optimality of these solutions is confirmed by computing the eigenvalues of the Hessian matrix. First, for random ground motion case, the set of equations given by Eq. (3.5) must be used as the objective functions in order to formulate the optimization problems that minimize the variances of the frequency response $|H_{M_s}(\Omega)|^2$ for each device. These optimization problems can be written as follow

$$\begin{cases} \min\limits_{\mu,q,\eta,\zeta_1,\zeta_2} \sigma^2_{DVAs-Parallel}(\beta_1,\mu,q,\eta,\zeta_1,\zeta_2) \\ \min\limits_{\mu,q,\eta,\zeta_2} \sigma^2_{DVAs-series}(\beta_1,\mu,q,\eta,\zeta_2) \\ \min\limits_{\alpha,q,\eta,\zeta_1} \sigma^2_{2dof-TVA}(\beta,\alpha,q,\eta,\zeta_1) \\ \min\limits_{\mu,q,\eta,\zeta_1} \sigma^2_{IDVA-C6}(\beta,\mu,q,\eta,\zeta_1) \\ \min\limits_{\mu,q,\eta,\zeta_1} \sigma^2_{IDVA-C4}(\beta,\mu,q,\eta,\zeta_1) \\ \min\limits_{\mu,q,\eta,\zeta_1} \sigma^2_{IDVA-C3}(\beta,\mu,q,\eta,\zeta_1) \\ \quad Subject\ \ to \\ \{\mu,\alpha,q,\eta,\zeta_1,\zeta_2\} \geq 0 \end{cases} \tag{3.7}$$

In order to validate the optimality of optimal solutions μ_{opt}, α_{opt}, q_{opt}, η_{opt}, $\zeta_{1,opt}$, and $\zeta_{2,opt}$ provided by Maplesoft, the eigenvalues of the Hessian matrix can be used to determine the global and local minimum conditions at these solutions. In a general way, the Hessian matrix evaluated at these solutions can be written as follows

$$H(\sigma_i^2) = \nabla^2(\sigma_i^2) = \begin{bmatrix} \frac{\partial^2\sigma_i^2}{\partial\mu^2} & \frac{\partial^2\sigma_i^2}{\partial\mu\partial\alpha} & \frac{\partial^2\sigma_i^2}{\partial\mu\partial q} & \frac{\partial^2\sigma_i^2}{\partial\mu\partial\eta} & \frac{\partial^2\sigma_i^2}{\partial\mu\partial\zeta_1} & \frac{\partial^2\sigma_i^2}{\partial\mu\partial\zeta_2} \\ \frac{\partial^2\sigma_i^2}{\partial\alpha\partial\mu} & \frac{\partial^2\sigma_i^2}{\partial\alpha^2} & \frac{\partial^2\sigma_i^2}{\partial\alpha\partial q} & \frac{\partial^2\sigma_i^2}{\partial\alpha\partial\eta} & \frac{\partial^2\sigma_i^2}{\partial\alpha\partial\zeta_1} & \frac{\partial^2\sigma_i^2}{\partial\alpha\partial\zeta_2} \\ \frac{\partial^2\sigma_i^2}{\partial q\partial\mu} & \frac{\partial^2\sigma_i^2}{\partial q\partial\alpha} & \frac{\partial^2\sigma_i^2}{\partial q^2} & \frac{\partial^2\sigma_i^2}{\partial q\partial\eta} & \frac{\partial^2\sigma_i^2}{\partial q\partial\zeta_1} & \frac{\partial^2\sigma_i^2}{\partial q\partial\zeta_2} \\ \frac{\partial^2\sigma_i^2}{\partial\eta\partial\mu} & \frac{\partial^2\sigma_i^2}{\partial\eta\partial\alpha} & \frac{\partial^2\sigma_i^2}{\partial\eta\partial q} & \frac{\partial^2\sigma_i^2}{\partial\eta^2} & \frac{\partial^2\sigma_i^2}{\partial\eta\partial\zeta_1} & \frac{\partial^2\sigma_i^2}{\partial\eta\partial\zeta_2} \\ \frac{\partial^2\sigma_i^2}{\partial\zeta_1\partial\mu} & \frac{\partial^2\sigma_i^2}{\partial\zeta_1\partial\alpha} & \frac{\partial^2\sigma_i^2}{\partial\zeta_1\partial q} & \frac{\partial^2\sigma_i^2}{\partial\zeta_1\partial\eta} & \frac{\partial^2\sigma_i^2}{\partial\zeta_1^2} & \frac{\partial^2\sigma_i^2}{\partial\zeta_1\partial\zeta_2} \\ \frac{\partial^2\sigma_i^2}{\partial\zeta_2\partial\mu} & \frac{\partial^2\sigma_i^2}{\partial\zeta_2\partial\alpha} & \frac{\partial^2\sigma_i^2}{\partial\zeta_2\partial q} & \frac{\partial^2\sigma_i^2}{\partial\zeta_2\partial\eta} & \frac{\partial^2\sigma_i^2}{\partial\zeta_2\partial\zeta_1} & \frac{\partial^2\sigma_i^2}{\partial\zeta_2^2} \end{bmatrix} \tag{3.8}$$

In Eq. (3.8) σ_i^2 corresponds to each variance given by the Eqs. (3.5) and (3.6). The eigenvalues can be computed by solving the following equation

$$|\lambda_i\mathbf{I} - \nabla^2(\sigma_i^2)| = 0 \tag{3.9}$$

where λ_i are the eigenvalues of the Hessian matrix $H(\sigma_i^2)$. For both excitation cases, the optimality of these optimal solutions was verified by Eq. (3.9), and eigenvalues are all positive at μ_{opt}, α_{opt}, q_{opt}, η_{opt}, $\zeta_{1,opt}$, and $\zeta_{2,opt}$, see figures in Appendix B. It means that the variances σ_i^2 reach a global minimal at these points.

Then, for random force excitation case, the Eq. (3.6) are objective functions to be minimized, and the formulation of the optimization problems is similar to the random ground motion case. For both excitation cases, the optimization problems given by the Eq. (3.7) do not have inequality and equality constraints which became in unconstrained nonlinear optimization problems. Then, the optimal parameters for the optimal design for each device can be obtained by solving these optimization problems by means of command *NLPSolve* provided by MapleSoft. The *NLPSolve* command solves a nonlinear program (NLP), which involves computing the minimum (or maximum) of a real-valued objective function, possibly subject to constraints. Generally, a local minimum is returned unless the problem is convex. The methods used by the *NLPSolve* command are Modified Newton, Preconditioned Conjugate Gradient (PCG), and Sequential Quadratic Programming (SQP) [74]. Although this command has powerful solvers, it will always be a blackbox for optimization. In order to demonstrate the convexity for the optimization problems defined before, the Hessian matrix and the eigenvalues were computed. By using this

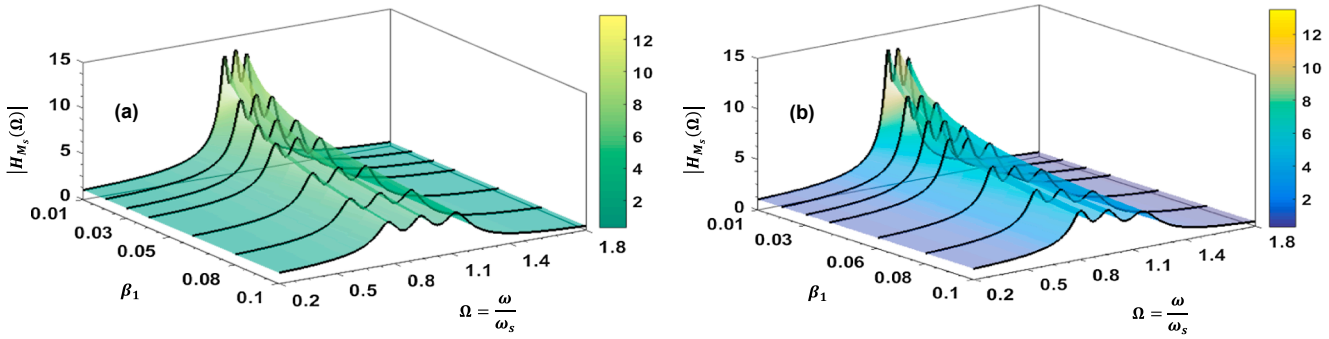

Fig. 3.1. Optimal frequency response curves for DVAs arranged in parallel: (a) random ground motion excitation; (b) random force excitation.

approach, the mass ratios β_1 for 1%, 3%, 5%, 7%, and 10% are considered to determine the optimal design for the parallel-type DVAs. These mass ratios were selected because in practice applications the size of DVAs must be small for space-installation issues. Therefore, the optimal frequency response curves for the DVAs arranged in parallel under the effect of random ground motion and force excitation are depicted in Fig. 3.1(a) and (b), respectively.

In Fig. 3.1(a) and (b) can be seen frequency response curves present three resonant peaks. This extra peak is presented because the parallel-type DVAs is a three degree-of-freedom mechanical system and has the effect of widening the effective operating bandwidth of this device. It means that the DVAs arranged in parallel can attenuate other lower and higher external excitation frequencies due to use two resonant vibration modes, unlike the classic DVA only use one resonant mode. Additionally, some optimal parameters for these numerical simulations are shown in Table 3.1.

Additionally, for both excitation cases, the optimal parameter curves for μ_{opt}, q_{opt}, η_{opt}, $\zeta_{1,opt}$, and $\zeta_{2,opt}$ that minimize the variances of squared modulus of the FRF $|H(j\Omega)|^2$ for this device are shown in Appendix B, see Figs. 8.1 and 8.2(a–d). Similarly, for the optimal design of DVA arranged in series, the variances $\sigma^2_{DVAs-series}(\beta_1, \mu, q, \eta, \zeta_2)$ of each equation (3.5) and (3.6) must be minimized. Then, by using the proposed mass ratios β_1, the values for the optimal design of this device are shown in Table 3.2. Hence, the optimal frequency response curves for the DVAs arranged in series subjected to random ground motion and force excitation are depicted in Fig. 3.2(a) and (b), respectively.

For both excitation cases, both frequency response curves and vibration amplitudes of DVAs arranged in series are flatter and minimal than those of DVAs arranged in parallel, and minimum variance values σ^2_{min} of DVAs arranged in series showed in Table 3.2 are smaller than those depicted in Table 3.1 of the parallel-type DVAs. In fact, a minimal variance also indicates that the standard deviation of the displacement in frequency domain of primary structure is minimal [10]. It means that frequency response of the system is also minimal. For the measurement of relative improvement between the dynamic performance of the DVAs connected in series and DVAs arranged in parallel is necessary to define the following relative dynamic performance (RDP)

$$\%\text{RDP} = \left(\frac{||H_{DVAs-parallel}(j\Omega)||_2^2\text{norm} - ||H_{DVAs-series}(j\Omega)||_2^2\text{norm}}{||H_{DVAs-parallel}(j\Omega)||_2^2\text{norm}}\right)100\% = \left(\frac{\sigma^2_{min,DVAs-parallel}(\beta_1, \mu_{opt}, q_{opt}, \eta_{opt}, \zeta_{1,opt}, \zeta_{2,opt}) - \sigma^2_{min,DVAs-series}(\beta_1, \mu_{opt}, q_{opt}, \eta_{opt}, \zeta_{2,opt})}{\sigma^2_{min,DVAs-parallel}(\beta_1, \mu_{opt}, q_{opt}, \eta_{opt}, \zeta_{1,opt}, \zeta_{2,opt})}\right)100\% \tag{3.10}$$

In Eq. (3.10), the minimal variance values $\sigma^2_{min,DVAs-series}$ and $\sigma^2_{min,DVAs-parallel}$ are shown in Table 3.2 and Table 3.1, respectively. Therefore, for the mass ratio range $0.01 \leq \beta \leq 0.1$, DVAs arranged in series presents more than 7.53% improvement with respect to the DVA arranged in parallel for the random ground motion excitation case. In addition, for random force excitation case, the DVAs arranged in series provides a 7.36–6.93% improvement with respect to the DVAs connected in parallel, which means that RDP of DVAs in series decreases. Additionally, the optimal parameter curves μ_{opt}, q_{opt}, η_{opt}, and $\zeta_{2,opt}$ for design of the series-type DVAs are depicted in Appendix B.

Additionally, for the optimization of 2dof TVA with translational and rotational motion, the variances $\sigma^2_{2dof-TVA}(\beta, \alpha, q, \eta, \zeta_1)$ given by Eqs. (3.5) and (3.6) need to be minimized which can be performed through the formulation (3.7). From proposed mass ratio β 1%, 3%, 5%, 7%, and 10%, the optimal parameters that minimize the variance for FRF $|H(j\Omega)|^2$ of primary structure are α_{opt}, q_{opt}, η_{opt}, and $\zeta_{1,opt}$. By solving for these mass ratios, the optimal frequency response curves for the 2dof TVA with translational and rotational motion subjected to random

Table 3.1
Optimal parameters for the optimum design of parallel-type DVAs.

β_1	μ_{opt}	q_{opt}	η_{opt}	$\zeta_{1,opt}$	$\zeta_{2,opt}$	σ^2_{min}
(a) random ground motion excitation						
0.01	0.8724	0.9576	1.0690	0.0313	0.0308	9.4826
0.03	0.7913	0.9162	1.1232	0.0544	0.0527	5.6233
0.05	0.7415	0.8834	1.1625	0.0702	0.0673	4.4714
0.07	0.7044	0.8545	1.1960	0.0830	0.0790	3.8772
0.10	0.6618	0.8157	1.2402	0.0989	0.0933	3.3678
(b) random force excitation						
0.01	0.9375	0.9628	1.0686	0.0308	0.0313	9.3490
0.03	0.8948	0.9314	1.1210	0.0529	0.0542	5.3918
0.05	0.8669	0.9083	1.1578	0.0678	0.0698	4.1721
0.07	0.8453	0.8888	1.1879	0.0796	0.0824	3.5225
0.10	0.8193	0.8636	1.2261	0.0941	0.0981	2.9428

Table 3.2
Optimal parameters for optimum design of the DVAs arranged in series considering $\zeta_1 = 0$.

β_1	μ_{opt}	q_{opt}	η_{opt}	$\zeta_{2,opt}$	σ^2_{min}
(a) random ground motion excitation					
0.01	0.0201	1.0025	0.9802	0.0861	8.7685
0.03	0.0613	1.0076	0.9419	0.1478	5.1877
0.05	0.1037	1.0127	0.9053	0.1889	4.1155
0.07	0.1473	1.0179	0.8702	0.2215	3.5605
0.10	0.2148	1.0258	0.8205	0.2612	3.0823
(b) random force excitation					
0.01	0.0199	1.0099	0.9803	0.0857	8.6602
0.03	0.0600	1.0295	0.9433	0.1456	4.9999
0.05	0.0999	1.0488	0.9090	0.1846	3.8729
0.07	0.1400	1.0677	0.8771	0.2145	3.2732
0.10	0.1999	1.0954	0.8333	0.2499	2.7386

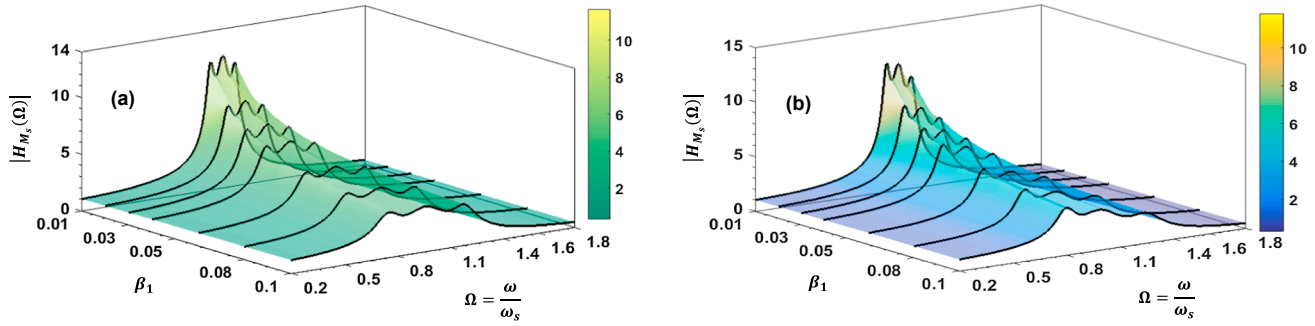

Fig. 3.2. Optimal frequency response curves for DVAs arranged in series: (a) random ground motion excitation; (b) random force excitation.

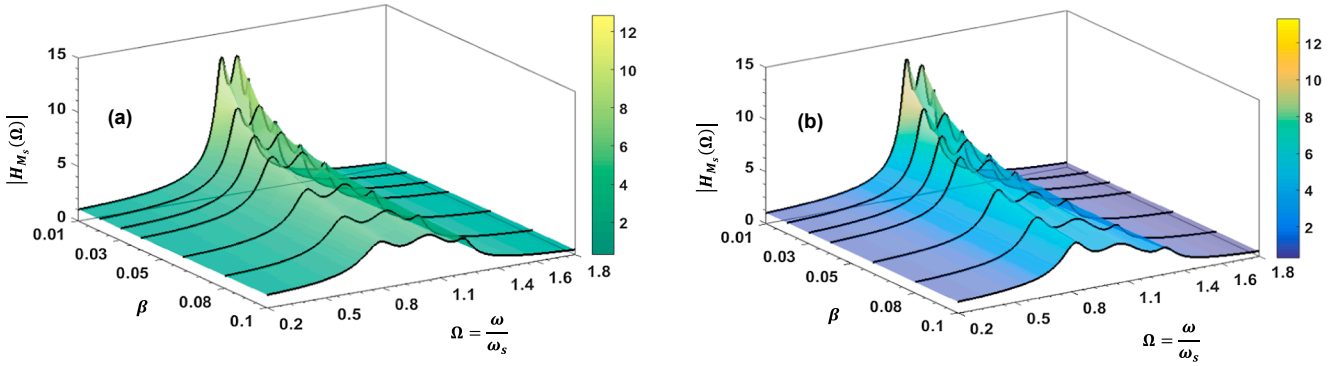

Fig. 3.3. Optimal frequency response curves for 2dof TVA with translational and rotational motion: (a) random ground motion excitation; (b) random force excitation.

ground motion and force excitation are described in Fig. 3.3(a) and (b), respectively.

The optimal parameters α_{opt}, q_{opt}, η_{opt}, and $\zeta_{1,opt}$ of the 2dof TVA are shown in Table 3.3, and optimal curves for these parameters are depicted in Appendix B. For both excitation cases, note that the optimal FRFs of this device are quite similar to those of the DVAs arranged in parallel or series, see Fig. 3.1, Fig. 3.2, and Fig. 3.3. Indeed, translation and rotation motions of the 2dof TVA yield two resonant vibration modes that have effect of broadening the FRFs curves of this device. On the other hand, note that the variances of the DVAs arranged in series are minor than those of the 2dof TVA, see Table 3.2 and Table 3.3. By substituting the minimal variances computed from the mass ratios $0.01 \leq \beta \leq 0.1$, relative RDPs between DVAs in series and 2dof TVA are 5.51–3.85% and 5.84–4.32% for random ground motion and random force excitation, respectively. It means that the DVA arranged in series is more effective for mitigating of vibration than 2dof TVA for both random excitation cases. Additionally, the 2dof TVA yields a RDP of 2.13–4.80% and 1.61–2.73% with respect to the DVAs arranged in parallel for random ground motion and random force excitation, respectively, which the 2dof TDVA presents major effectiveness than the another one. Besides, for small mass ratio values for $0.01 < \beta$, the optimal radius ratio $1/\sqrt{\alpha_{opt}} = \rho/d$ is approximated to be the unit, and the behavior of the 2dof TVA is like the DVAs arranged in parallel. However, for mass ratio values $\beta \geq 0.05$, the 2dof TVA presents more dynamic performance than parallel-type DVAs.

Table 3.3
Optimal parameters for the optimum design TVA with translational and rotational motion considering $\zeta_2 = 0$.

β	$1/\sqrt{\alpha_{opt}} = \rho/d$	q_{opt}	η_{opt}	$\zeta_{1,opt}$	σ^2_{min}
(a) random ground motion excitation					
0.01	0.8992	0.6664	1.0619	0.0468	9.2806
0.03	0.8253	0.6259	1.1152	0.0805	5.4549
0.05	0.7751	0.5938	1.1567	0.1032	4.3098
0.07	0.7349	0.5657	1.1939	0.1213	3.7169
0.10	0.6854	0.5285	1.2460	0.1437	3.2059
(b) random force excitation					
0.01	0.9000	0.6707	1.0630	0.0460	9.1980
0.03	0.8281	0.6386	1.1177	0.0779	5.2821
0.05	0.7801	0.6148	1.1598	0.0986	4.0760
0.07	0.7423	0.5948	1.1967	0.1146	3.4342
0.10	0.6965	0.5692	1.2466	0.1336	2.8623

Finally, for this optimization part, the dynamic performance for inerter-based DVAs is analyzed when subjected to the random ground motion and force excitation. In a recent research, numerical solutions for the optimal design of these devices have been derived under the effect of random force excitation [49]; However, when the excitation source in mechanical structures are earthquakes, the random ground motion excitation is more convenient to analyze than the other ones [71]. In this paper, optimal curves for μ_{opt}, q_{opt}, η_{opt}, and $\zeta_{1,opt}$ are numerically computed for design of IDVAs subjected to the random ground motion excitation, and they are depicted in Appendix B. First, for both random excitation sources, the variances $\sigma^2_{IDVA-C6}(\beta, \mu, q, \eta, \zeta_1)$ for IDVA-C6 provided by Eqs. (3.5) and (3.6) are considered to the formulation of optimization problems. Considering the mass ratio β 1%, 3%, 5%, 7%, and 10%, the optimal parameters μ_{opt}, q_{opt}, η_{opt},and $\zeta_{1,opt}$ that yield a minimal variance are computed by Maplesoft and shown in Table 3.4. Therefore, the optimal FRF curves for the inerter-based dynamic vibration absorber (IDVA-C6) subject to the two random excitation cases are depicted in Fig. 3.4(a) and (b), respectively.

Note that the minimal values for variances $\sigma^2_{IDVA-C6}(\beta, \mu, q, \eta, \zeta_1)$ are exactly equal to those of the DVAs arranged in series, which means that these devices have the same dynamic performance index, see Table 3.2 and Table 3.4. On the other hand, for small values of μ, the dynamic behavior of the IDVA-C6 is similar to that of the Three-Element DVA [4]. It is obvious because by setting the inertance value of $b = 0$ in the mechanical impedance C6 showed in Fig. 2.2, the result is a series connection of a spring and a damper which is the definition for Three-Element DVA. When the minimal variance values of IDVA-C6 are compared with respect to those of the 2dof TVA with translational and

Table 3.4
Optimal parameters for the optimum design of the IDVA-C6.

β	μ_{opt}	q_{opt}	η_{opt}	$\zeta_{1,opt}$	σ^2_{min}
(a) random ground motion excitation					
0.01	0.0193	0.9827	1.0201	0.0017	8.7685
0.03	0.0545	0.9493	1.0610	0.0085	5.1877
0.05	0.0853	0.9175	1.1030	0.0178	4.1155
0.07	0.1125	0.8870	1.1460	0.0285	3.5605
0.10	0.1470	0.8439	1.2124	0.0465	3.0823
(b) random force excitation					
0.01	0.0192	0.9901	1.0199	0.0016	8.6602
0.03	0.0533	0.9712	1.0600	0.0082	4.9999
0.05	0.0826	0.9534	1.1000	0.0167	3.8729
0.07	0.1077	0.9365	1.1400	0.0263	3.2732
0.10	0.1388	0.9128	1.2000	0.0416	2.7386

Table 3.5
Optimal parameters for the optimum design of the IDVA-C4.

β	μ_{opt}	q_{opt}	η_{opt}	$\zeta_{1,opt}$	σ^2_{min}
(a) random ground motion excitation					
0.01	0.0194	0.9899	0.9906	0.0016	8.8041
0.03	0.0555	0.9698	0.9748	0.0074	5.2481
0.05	0.0888	0.9498	0.9618	0.0145	4.1923
0.07	0.1200	0.9302	0.9508	0.0221	3.6503
0.10	0.1635	0.9014	0.9368	0.0337	3.1884
(b) random force excitation					
0.01	0.0193	0.9973	0.9905	0.0016	8.6808
0.03	0.0551	0.9913	0.9742	0.0074	5.0325
0.05	0.0877	0.9848	0.9605	0.0145	3.9115
0.07	0.1177	0.9779	0.9485	0.0220	3.3155
0.10	0.1590	0.9672	0.9330	0.0335	2.7840

Table 3.6
Optimal parameters for the optimum design of the IDVA-C3.

β	μ_{opt}	q_{opt}	η_{opt}	$\zeta_{1,opt}$	σ^2_{min}
(a) random ground motion excitation					
0.01	0.0199	0.9863	1.0049	0.0576	8.7739
0.03	0.0592	0.9598	1.0149	0.0996	5.1972
0.05	0.0979	0.9343	1.0248	0.1284	4.1279
0.07	0.1362	0.9097	1.0347	0.1517	3.5753
0.10	0.1926	0.8743	1.0495	0.1809	3.1002
(b) random force excitation					
0.01	0.0198	0.9938	1.0049	0.0574	8.6584
0.03	0.0583	0.9817	1.0148	0.0984	4.9969
0.05	0.0955	0.9701	1.0246	0.1257	3.8691
0.07	0.1313	0.9588	1.0343	0.1472	3.2688
0.10	0.1828	0.9426	1.0487	0.1734	2.7334

rotational, the RDPs are 5.51–3.85% and 5.84–4.32% for random ground motion and random force excitation, respectively. Note that the previously obtained RDPs are quite similar to those obtained through comparison of the relative dynamic performance between the DVAs arranged in series and 2dof TVA. In addition, the relative dynamic performance of the IDVA-C6 outperforms to that of the DVA arranged in parallel by approximately 7%, which is easy to note.

For the optimization of the DVAs C4 and C3, the variances $\sigma^2_{IDVA-C4}(\beta, \mu, q, \eta, \zeta_1)$ and $\sigma^2_{IDVA-C3}(\beta, \mu, q, \eta, \zeta_1)$ need to be minimized. From the set of Eqs. (3.5) and (3.6), unconstrained nonlinear optimization problems can be formulated using (3.7), which are then solved by means of Maplesoft global optimization toolbox. Therefore, for the proposed mass ratios, optimal parameters μ_{opt}, q_{opt}, η_{opt}, and $\zeta_{1,opt}$ that yield minimal variances $\sigma^2_{min,IDVA-C4}(\beta, \mu, q, \eta, \zeta_1)$ and $\sigma^2_{min,IDVA-C3}(\beta, \mu, q, \eta, \zeta_1)$ are shown in Table 3.5 and Table 3.6. For both random excitation cases, optimal FRFs curves for the IDVAs C4 and C3 are depicted in Fig. 3.5 and Fig. 3.6(a) and (b), respectively.

Note that, for mass ratio values of $0.01 \leq \beta \leq 0.1$, the IDVA-C3 presents 0.34–2.76% of RDP (relative dynamic performance) with respect to the IDVA-C4 considering the minimal variances of random ground motion excitation case showed in Table 3.5 and Table 3.6. For random force excitation case, the IDVA-C3 yields 0.25–1.81% of improvement with respect to the IDVA-C4. In addition, by comparing the minimal variances of the IDVA-C3 with those of the IDVA-C6 showed in Table 3.4, the IDVA-C6 presents a relative improvement from 0.061 to 0.57% when is compared with the IDVA-C3 for random ground excitation case. For random force excitation case, the IDVA-C3 yields 0.02–0.18% of RDP with respect to the IDVA-C6. This means that IDVA-C3 presents major effectiveness for suppressing vibration than IDVA-C6 for random force excitation case, however the IDVA-C6 is better for random ground motion excitation case. This affirmation will be claimed in Section 3.2 by means of comparison of the relative dynamic performance (RDP) between the types of high-performance passive DVAs studied is this research and the classic DVA. Therefore, the IDVA-C6, DVAs arranged in series, and IDVA-C3 are better effective for attenuating vibration than the IDVA-C4, and consequently the IDVA-C4 presents major relative dynamic performance than the 2dof TVA and DVAs arranged in parallel.

In the next subsection, a numerical simulation is performed considering the mass ratio $\beta = 10\%$ in order to compare the optimal FRFs curves of all devices studied in this work. Since the IDVA-C6 has the same dynamic performance than DVAs arranged in series, the optimal FRFs curves of these devices will demonstrate equal dynamic behavior. Then, the relative dynamic performance (RDP) is computed through Eq. (3.10) to compare the effectiveness of these types of high-performance passive DVAs with respect to the classic DVA. Additionally, the widening percentages of the effective operating bandwidth of these devices is also compared with respect to the classic DVA.

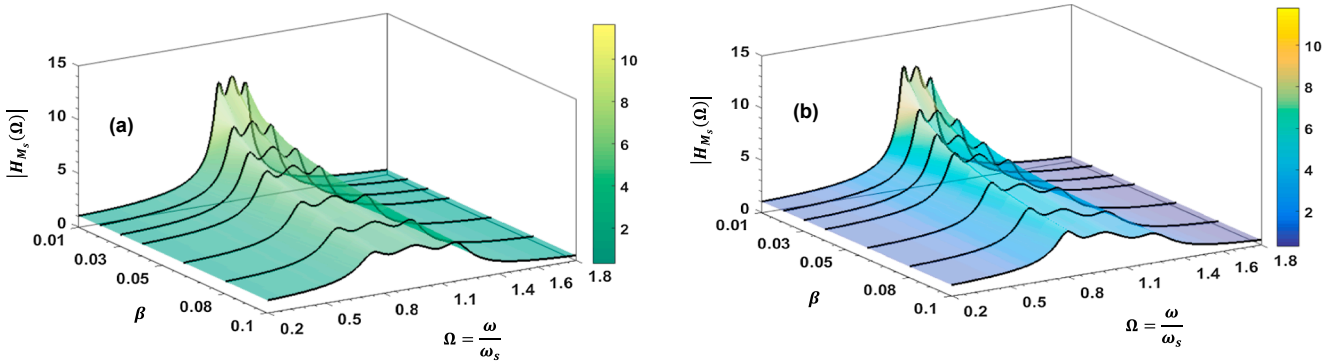

Fig. 3.4. Optimal frequency response curves for IDVA-C6: (a) random ground motion excitation; (b) random force excitation.

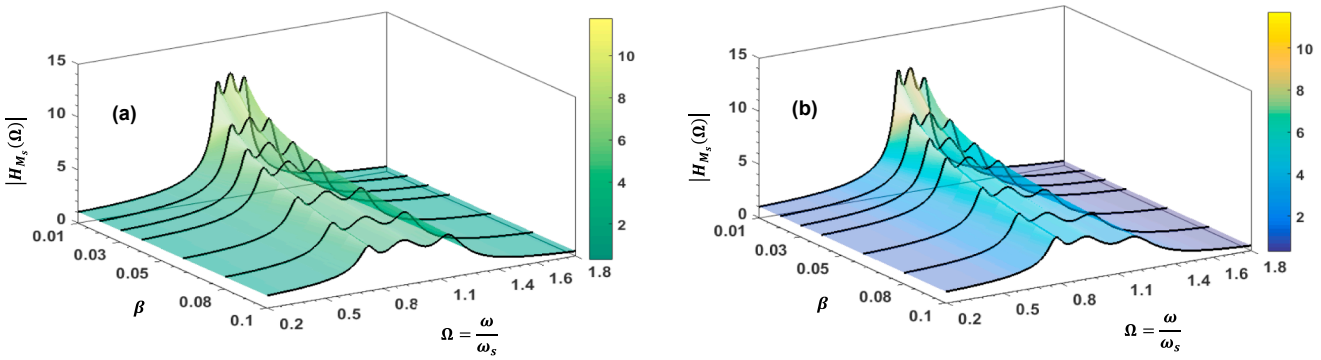

Fig. 3.5. Optimal frequency response curves for IDVA-C4: (a) random ground motion excitation; (b) random force excitation.

3.2. Comparison of performances for all devices

In this subsection, the optimal FRF curves of all devices depicted in Fig. 2.1(a), (b), (c) and Fig. 2.2 are obtained considering the mass ratio $\beta = 10\%$ in order to compare the dynamic performance of these devices with respect to that of the classic DVA. These optimal FRFs are shown in Fig. 3.7(a) and (b) for both excitation cases.

In Fig. 3.7(a) and (b) can be seen that both DVAs arranged in series and IDVA-C6 have the same optimal FRF curve, that is, these devices present the same vibration amplitudes at all excitation frequencies. It means that IDVA-C6 can be replaced by the DVAs arranged in series because the IDVA-C6 has the same dynamic performance than the DVAs-series. In some investigations, the IDVA-C6 is called as the rotational inertial double tuned mass damper [60,62]. Note that the DVAs arranged in series is less expensive than the IDVA-C6 in terms of manufacturing and implementation for the passive vibration control. In addition, the DVAs connected in series could be more feasible for mitigating vibration into machining process than IDVA-C6 because the mounting space into that process is extremely reduced, and the installation either IDVA-C6 or an inerter is not possible. Indeed, the authors of [29] used a 2dof TVA for milling vibration mitigation, and the mounting space of the 2dof TVA is very small. Additionally, the minimal variance values σ^2_{min} for each device are depicted in Fig. 3.8.

According to the Table 3.2, Table 3.4, and Fig. 3.8(a) and (b) can be noted both IDVA-C6 and DVAs arranged in series have the same variance values or performance index σ^2_{min}. Although the IDVA-C6 has the advantage for yielding high apparent mass or inertance without modifying the physical size of inerter, the DVAs connected in series and 2dof TVA could be more appropriate for attenuating vibration in systems with very reduced installation space; However, the IDVA-C6 is feasible to use in mounting space bigger than that used into milling process. Additionally, the relative dynamic performance (RDP) percentages for each device are computed from Eq. (3.10) and compared with respect to that of the classic DVA, see Table 3.7.

According to the Table 3.7, it was found that both DVAs arrange in series and IDVA-C6 have the same relative dynamic performance ($\%\text{RDP}_{DVAs-series} = \%\text{RDP}_{IDVA-C6}$), which is major to the 13.50% and minor to the 13.29% for random ground motion and force excitation case, respectively. Moreover, for random ground motion excitation case, the performance of the IDVA-C4 decrease by increasing the value of β, while the performance of the 2dof TVA with translational and rotational motion increases. In excitation case (a), the devices that yield more dynamic performance than classic DVA are the following: the DVAs arranged in series, IDVA-C6, IDVA-C3 or $\%\text{RDP}_{DVAs-series} = \%\text{RDP}_{IDVA-C6} > \%\text{RDP}_{IDVA-C3}$. Besides, for the random force excitation, the IDVA-C3 yields major performance while the DVAs arranged in series and IDVA-C6 have the same dynamic performance or $\%\text{RDP}_{IDVA-C3} > \%\text{RDP}_{DVAs-series} = \%\text{RDP}_{IDVA-C6}$. In addition, for this excitation case, it can be noted that the performance of the IDVA-C4 decrease by increasing the value of β while the performance of the 2dof TVA increases.

In Fig. 3.9(a) can be noted that DVAs connected in series, IDVA-C6, and IDVA-C3 can provide more than 13% improvement with respect to the classic DVA. On the other hand, in Fig. 3.9(b) can be seen that these devices yield more than 10% improvement when are compared with the classic DVA.

In addition, the effective operating range or suppression band index (SB_i) can be defined as the range of excitation frequencies in which the primary structure controlled either the high-performance DVAs studied is this paper or a classic DVA outperforms an uncontrolled structure. By using the magnitudes $\text{SB}_{classic\ \ DVA}$, $\text{SB}_{DVAs-parallel}$, $\text{SB}_{DVAs-series}$, $\text{SB}_{2dof-TVA}$, $\text{SB}_{IDVA-C6}$, $\text{SB}_{IDVA-C4}$, and $\text{SB}_{IDVA-C3}$ depicted in Fig. 3.7(a) and (b), the suppression band index can be computed as $\%\text{SB}_i = \left(\frac{SB_{types\ \ DVAs} - SB_{classic\ \ DVA}}{SB_{classic\ \ DVA}}\right)100\%$. From this definition, the $\%\text{SB}_i$ for these devices are shown in Fig. 3.10(a) and (b) for both excitation cases.

Note that in Fig. 3.10(a) and (b) the 2dof-TVA, IDVA-C6, C4, C3, and DVAs connected in series present more than 30% of widening of effective operating range with respect to the classic DVA. It means that these devices are more effective and robust for mitigating vibration

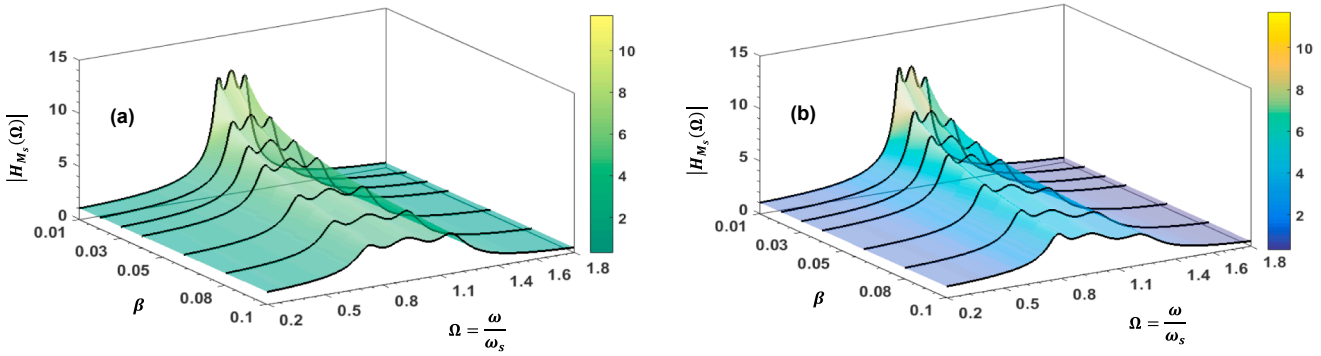

Fig. 3.6. Optimal frequency response curves for IDVA-C3: (a) random ground motion excitation; (b) random force excitation.

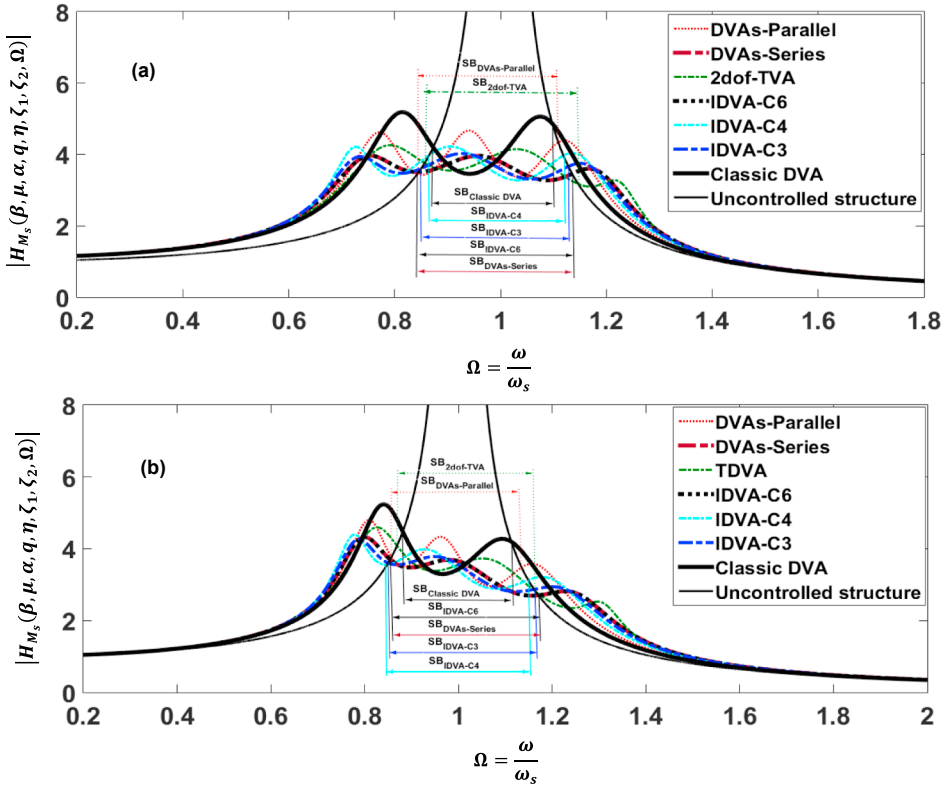

Fig. 3.7. Comparison of optimal frequency response curves for absorbers studied in this paper with respect to that of the classic DVA considering the ratio $\beta = 10\%$: (a) random ground motion excitation case; (b) random force excitation case.

around resonance than classic DVA. Indeed, that affirmation can be noted in Fig. 3.10(a) and (b) in which the vibration amplitudes around resonance are smaller than that of the classic DVA. However, for forced frequency ratios Ω below 0.85 and over 1.15, the classic DVA and uncontrolled structure outperform to the high-performance DVAs. This inconvenient can be avoided by correctly tuning these devices.

In the next section, the H_∞ optimization is performed in order to corroborate that the DVAs arranged in series, IDVA-C6, and the IDVA-C3 present a dynamic behavior quite similar.

4. H_∞ Optimization

The target of H_∞ optimization method is to minimize the maximum vibration amplitude of frequency response $|H_{DVAs-parallel}(\Omega)|$, $|H_{DVAs-series}(\Omega)|$, $|H_{2dof-TVA}(\Omega)|$, and the $|H_{IDVAs}(\Omega)|$ (IDVAs C6, C4, and C3) at resonance frequencies, which is well known as the norm $||H(j\Omega)||_\infty$ [49,75]. Recently, quasi-optimal solutions were obtained for the IDVAs C6, C4, and C3 from the invariant frequencies of frequency response of the main structure [69]. This optimization process is called as the extended fixed-points technique which is analogous to the H_∞ optimization method. Note that, both the DVAs arranged in series and 2dof TVA with translational and rotational motion have four invariant frequencies look like to those of the IDVA-C6, C4, and C3. Nevertheless, the DVAs arranged in parallel does not has invariant frequencies, and the extended fixed-points technique cannot be applied for the optimization of this device [66]. Hence, numerical solutions for the optimal design for devices showed in Fig. 2.1(a), (b), (c), and Fig. 2.2 can be obtained by formulating the H_∞ optimization problem, which can be written as.

$$\begin{cases} \max(|H_{DVAs-parallel}(\mu_{opt}, q_{opt}, \eta_{opt}, \zeta_{1,opt}, \zeta_{2,opt}, \Omega)|) = \min(\max_{\mu,q,\eta,\zeta_1,\zeta_2}(|H_{DVAs-parallel}(\Omega)|)) \\ \max(|H_{DVAs-series}(\mu_{opt}, q_{opt}, \eta_{opt}, \zeta_{2,opt}, \Omega)|) = \min(\max_{\mu,q,\eta,\zeta_2}(|H_{DVAs-series}(\Omega)|)) \\ \max(|H_{2dof-TVA}(\alpha_{opt}, q_{opt}, \eta_{opt}, \zeta_{1,opt}, \Omega)|) = \min(\max_{\alpha,q,\eta,\zeta_1}(|H_{2dof-TVA}(\Omega)|)) \\ \max(|H_{DVA-C6}(\mu_{opt}, q_{opt}, \eta_{opt}, \zeta_{1,opt}, \Omega)|) = \min(\max_{\mu,q,\eta,\zeta_1}(|H_{IDVA-C6}(\Omega)|)) \\ \max(|H_{DVA-C4}(\mu_{opt}, q_{opt}, \eta_{opt}, \zeta_{1,opt}, \Omega)|) = \min(\max_{\mu,q,\eta,\zeta_1}(|H_{IDVA-C4}(\Omega)|)) \\ \max(|H_{DVA-C3}(\mu_{opt}, q_{opt}, \eta_{opt}, \zeta_{1,opt}, \Omega)|) = \min(\max_{\mu,q,\eta,\zeta_1}(|H_{IDVA-C3}(\Omega)|)) \end{cases} \quad (4.1)$$

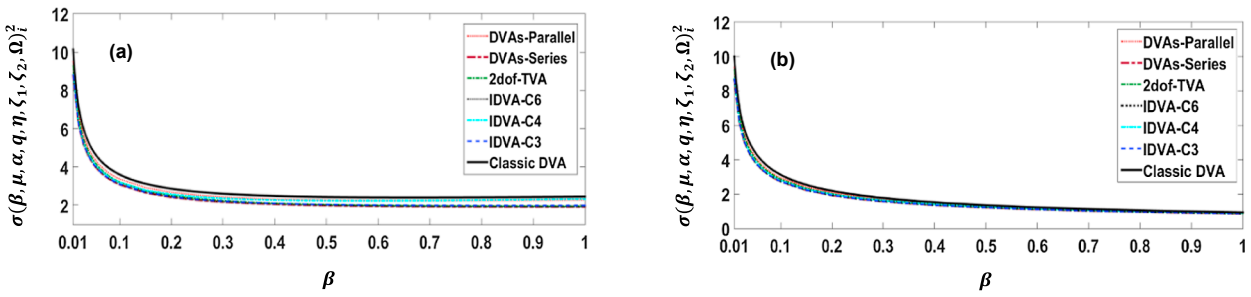

Fig. 3.8. Performance indexes for all devices: (a) random ground motion excitation; (b) random force excitation.

Table 3.7
Improvement percentages for high-performance DVAs compared with the classical DVA.

β	$\%\sigma^2_{DVAs-parallel}$	$\%\sigma^2_{DVAs-series}$	$\%\sigma^2_{2dof-TVA}$	$\%\sigma^2_{IDVA-C6}$	$\%\sigma^2_{IDVA-C4}$	$\%\sigma^2_{IDVA-C3}$
(a) RDP percentages for random ground motion excitation case						
0.01	6.4614	13.5052	8.4540	13.5052	13.1540	13.4516
0.03	6.4742	13.7180	9.2735	13.7180	12.7140	13.5599
0.05	6.4849	13.9273	9.8654	13.9273	12.3222	13.6681
0.07	6.4955	14.1331	10.3618	14.1331	11.9678	13.7763
0.10	6.5113	14.4356	11.0052	14.4356	11.4911	13.9387
(b) RDP percentages for random force excitation case						
0.01	6.3939	13.2901	7.9059	13.2901	13.0840	13.3080
0.03	6.2686	13.0804	8.1752	13.0804	12.5154	13.1330
0.05	6.1476	12.8773	8.3095	12.8773	12.0090	12.9634
0.07	6.0311	12.6805	8.3858	12.6805	11.5521	12.7988
0.10	5.8638	12.3963	8.4388	12.3963	10.9413	12.5609

where the FRFs $|H_{DVAs-parallel}(\Omega)|$, $|H_{DVAs-series}(\Omega)|$, $|H_{2dof-TVA}(\Omega)|$, and the $|H_{IDVAs}(\Omega)|$ are depicted in the Eq. (2.6), respectively. Solving the set of optimization problems given by the Eq. (4.1) for the mass ration $\beta = 10\%$ by means of the optimization method described in [4,67]. This optimization approach is mainly based on the observation of a trade-off relation among vibration amplitudes at resonant frequencies denoted by $|H(j\Omega_A)|$, $|H(j\Omega_B)|$, and $|H(j\Omega_C)|$, and then H_∞ performance index is defined as $||H(j\Omega)||_\infty = \max[|H(j\Omega_A)|, |H(j\Omega_B)|, |H(j\Omega_C)|]$. In order to compute the optimum performance measurement, Nishihara introduced a novel mathematical artifice in which the performance index can be expressed by $h = 1/\sqrt{1-r^2} = ||H(j\Omega)||_\infty$ [4]. The optimality approach of this methodology is strictly satisfied when the unknown r is minimized. On this assumption, the frequency response for each device can be expressed in terms of variable r. In fact, the optimum resonant frequencies can be also expressed by unknown variable r and therefore can be computed by solving a six-order polynomial. In order to achieve the same vibration amplitudes at resonance frequencies, the Vieta's theorem must be used which leads to an overdetermined nonlinear system of three high-order nonlinear equations. These nonlinear equations can be expressed as $f_i(\beta, \mu, \alpha, q, \eta, \zeta_1, \zeta_2, r) = 0$ *for* $i = 1, \cdots, 3$. To solve this system of simultaneous equations, constraint equations need to be added. These constraints provide a condition necessary to yield an optimal solution to the H_∞ criteria. Therefore, the remaining equations can be obtained by using the Jacobian matrix $J_f(\mu, \alpha, q, \eta, \zeta_1, \zeta_2) = \frac{\partial f_i(\mu,\alpha,q,\eta,\zeta_1,\zeta_2)}{\partial(\mu,\alpha,q,\eta,\zeta_1,\zeta_2)}$ of the infinitesimal variation of r with respect to the design parameters which are in implicit form $f_i(\beta, \mu, \alpha, q, \eta, \zeta_1, \zeta_2, r)$. Then, the optimality criteria approach is satisfied when any 3x3 minor determinant of the Jacobian matrix is equalized zero. Thus, this optimization methodology is summarized to numerically solve a set of high-order nonlinear equations which are the following

$$\left.\begin{aligned} &f_1(\beta,\mu,\alpha,q,\eta,\zeta_1,\zeta_2,r)=0\\ &f_2(\beta,\mu,\alpha,q,\eta,\zeta_1,\zeta_2,r)=0\\ &f_3(\beta,\mu,\alpha,q,\eta,\zeta_1,\zeta_2,r)=0\\ &\left|\frac{\partial(f_1,f_2,f_3)}{\partial(q,\eta,\zeta_2)}\right| = \begin{vmatrix} \frac{\partial f_1}{\partial q} & \frac{\partial f_1}{\partial \eta} & \frac{\partial f_1}{\partial \zeta_2}\\ \frac{\partial f_2}{\partial q} & \frac{\partial f_2}{\partial \eta} & \frac{\partial f_2}{\partial \zeta_2}\\ \frac{\partial f_3}{\partial q} & \frac{\partial f_3}{\partial \eta} & \frac{\partial f_3}{\partial \zeta_2} \end{vmatrix} = 0\\ &\left|\frac{\partial(f_1,f_2,f_3)}{\partial(\mu,q,\eta)}\right| = \begin{vmatrix} \frac{\partial f_1}{\partial \mu} & \frac{\partial f_1}{\partial q} & \frac{\partial f_1}{\partial \eta}\\ \frac{\partial f_2}{\partial \mu} & \frac{\partial f_2}{\partial q} & \frac{\partial f_2}{\partial \eta}\\ \frac{\partial f_3}{\partial \mu} & \frac{\partial f_3}{\partial q} & \frac{\partial f_3}{\partial \eta} \end{vmatrix} = 0\\ &\left|\frac{\partial(f_1,f_2,f_3)}{\partial(q,\eta,\zeta_1)}\right| = \begin{vmatrix} \frac{\partial f_1}{\partial q} & \frac{\partial f_1}{\partial \eta} & \frac{\partial f_1}{\partial \zeta_1}\\ \frac{\partial f_2}{\partial q} & \frac{\partial f_2}{\partial \eta} & \frac{\partial f_2}{\partial \zeta_1}\\ \frac{\partial f_3}{\partial q} & \frac{\partial f_3}{\partial \eta} & \frac{\partial f_3}{\partial \zeta_1} \end{vmatrix} = 0 \end{aligned}\right\} \forall\, \beta \in \mathrm{R}^+ \tag{4.2}$$

In addition, the optimality of the optimal solutions provided by solving the high-order nonlinear equations (4.2) can be also determined by computing the eigenvalues of Hessian matrix of the variation of DMF from frequency response evaluated at optimum resonant frequencies [69]. For the optimal design of the DVAs connected in parallel, the six equations given by equation (4.2) must be numerically solved using the Newton–Raphson method and thus the optimal parameters μ_{opt}, q_{opt}, η_{opt}, $\zeta_{1,opt}$, $\zeta_{2,opt}$, and $r_{min} = 0.9697$ are obtained. In addition, to achieve the rapid convergence of the solution method, the optimal parameters obtained from H_2 optimization criteria can be used as starting points. By solving the first five equations of Eq. (4.2), the

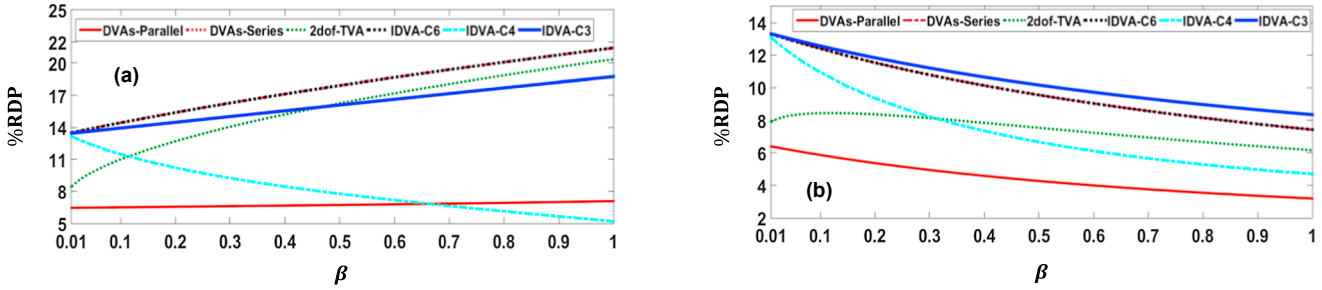

Fig. 3.9. Performance indexes for all devices: (a) random ground motion excitation case; (b) random force excitation case.

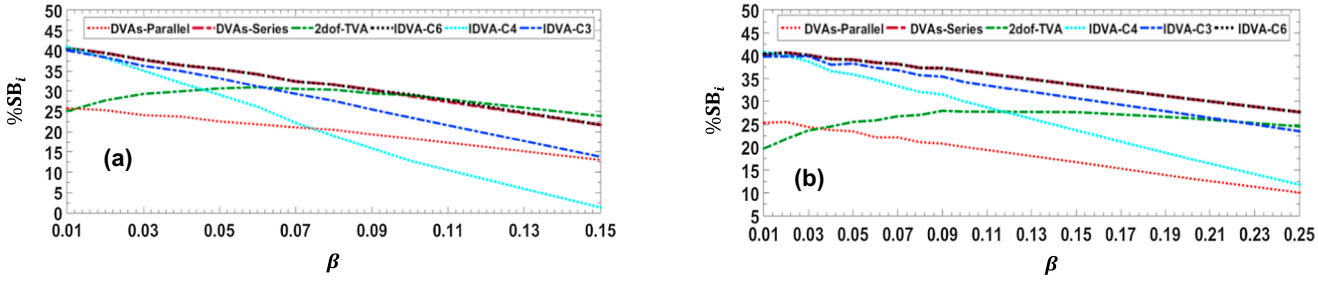

Fig. 3.10. Operating effective bandwidth index $\%SB_i = \left(\frac{SB_{types\ \ DVAs} - SB_{classic\ \ DVA}}{SB_{classic\ \ DVA}}\right)100\%$ for all devices: (a) random ground motion excitation case; (b) random force excitation case.

Table 4.1
Optimal parameters for all devices obtained by H_∞ optimization criteria.

(a) DVAs-parallel: solution in this paper						
β_1	μ_{opt}	q_{opt}	η_{opt}	$\zeta_{1,opt}$	$\zeta_{2,opt}$	$\|\|H(\Omega)\|\|_\infty$
0.10	0.7517	0.8473	1.2017	0.1227	0.1273	4.0963
(b) DVAs-series: solution in this paper						
β_1	μ_{opt}	q_{opt}	η_{opt}	$\zeta_{1,opt}$	$\zeta_{2,opt}$	$\|\|H(\Omega)\|\|_\infty$
0.10	0.2428	1.0723	0.8051	–	0.3132	3.6175
(c) TDVA with translational and rotational motion: solution in this paper						
β	$\frac{1}{\sqrt{\alpha_{opt}}}$	q_{opt}	η_{opt}	$\zeta_{1,opt}$	$\zeta_{2,opt}$	$\|\|H(\Omega)\|\|_\infty$
0.10	0.6606	0.5328	1.2272	0.1777	–	3.8108
(d) IDVA-C6 [49]						
β	μ_{opt}	q_{opt}	η_{opt}	$\zeta_{1,opt}$	$\zeta_{2,opt}$	$\|\|H(\Omega)\|\|_\infty$
0.10	0.1538	0.8642	1.2454	0.0593	–	3.6208
(e) IDVA-C4 [49]						
β	μ_{opt}	q_{opt}	η_{opt}	$\zeta_{1,opt}$	$\zeta_{2,opt}$	$\|\|H(\Omega)\|\|_\infty$
0.10	0.1930	0.9499	0.9013	0.0505	–	3.7448
(f) IDVA-C3 [49]						
β	μ_{opt}	q_{opt}	η_{opt}	$\zeta_{1,opt}$	$\zeta_{2,opt}$	$\|\|H(\Omega)\|\|_\infty$
0.10	0.2208	0.9083	1.0485	0.1657	–	3.6175

optimum variables μ_{opt}, q_{opt}, η_{opt}, $\zeta_{2,opt}$, and $r_{min} = 0.9610$ are provided for the optimum design of the DVA arranged in series. Then, for the optimum design for the 2dof-TVA, the variable μ must be replaced by α of the fifth equation of Eq. (4.2) in order to compute the optimal parameters α_{opt}, q_{opt}, η_{opt}, $\zeta_{1,opt}$ and $r_{min} = 0.9649$. These optimum parameters are given in Table 4.1. Finally, for optimum design of IDVAs, the first five equations of Eq. (4.2) can be solved however the optimal solutions have been provided in [49]. Therefore, it yields.

In Fig. 4.1(a) and (b) can be noted that both the DVAs arranged in series and IDVA-C6 have the same frequency response, which was observed in the H_2 optimization. However, the performances for these devices are different, which are $\|H_{DVAs-series}(\Omega)\|_\infty = 3.6175$ and $\|H_{IDVA-C6}(\Omega)\|_\infty = 3.6208$. In addition, the optimal parameters obtained via the H_∞ optimization are depicted in Table 4.1.

By introducing the concept of equivalent mass ratio provided in [4], interesting results are obtained. According to this concept is possible to compute an equivalent mass ratio of the traditional DVA that yields the same performance index than high-performance DVAs. For this purpose, closed-form performance index of traditional DVA is needed which can be written by following mathematical expression [75]

$$h_{max,classic\ \ DVA} = \|H(\Omega)\|_{\infty,classic\ \ DVA} = \frac{27\beta^2 + 80\beta + 64}{\sqrt{\beta((384\beta + 512)\sqrt{4 + 3\beta} + (9\beta + 16)(9\beta + 8)^2)}} \tag{4.3}$$

For example, by taking a mass ratio $\beta_1 = 0.1$ for DVAs connected in series, the performance index is $\|H(\Omega)\|_\infty = 3.6175$. The equivalent mass ratio β_{eq} for traditional DVA can be computed by substituting this performance index value into Eq. (4.3), and therefore $\beta_{eq} = 0.1662$. It means that the traditional DVA needs 66.2% additional mass to yield the same dynamic effect than DVAs arranged in series. When the performance indexes of 2dof-TVA and IDVA-C6 are considered, the equivalent mass ratios β_{eq} are 0.1485 and 0.1659; Therefore, the additional virtual masses are 48.5% and 65.9%, respectively. In fact, passive high-performance DVAs are better than traditional DVA.

Both DVAs arranged in series and IDVA-C3 have the same norm or performance $\|H_{DVAs-series}(\Omega)\|_\infty = \|H_{IDVA-C3}(\Omega)\|_\infty$, see Table 4.1. Note that, for $\|H(\Omega)\|_\infty$ criteria the DVAs arranged in series, IDVA-C6, and IDVA-C3 are better than other one. Besides, the optimal FRFs both DVAs arranged in series and IDVA-C6 obtained through the H_∞ and H_2 optimization are quite similar, see Fig. 3.7 and Fig. 4.1. It is very interesting that the IDVA-C6 known as the rotational inertial double tuned mass damper can be replaced by the DVAs arranged in series.

5. Conclusion

In this paper, the optimal design for high-performance Dynamic Vibration Absorbers was computed when subjected to random and harmonic vibration. These mechanical devices are the following; the DVAs arranged in parallel or series, 2dof-TVA with translational and

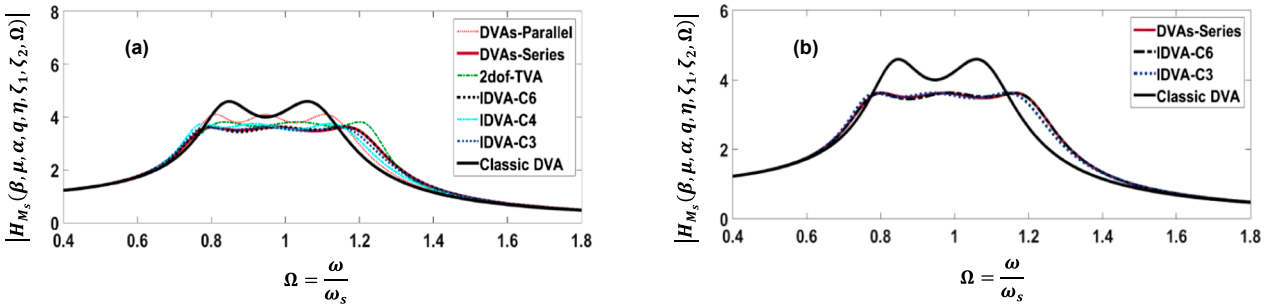

Fig. 4.1. H_∞ optimization for all devices: (a) Optimal FRFs curves for all devices considering the ratio $\beta = 10\%$; (b) comparison of optimal FRFs curves for the devices that provide more performance than other one.

rotational motion, and inerter-based dynamic vibrations absorbers (IDVAs). These types of DVAs use two resonant modes for suppressing the vibration of the dominant mode of the primary structure and have the effect of widening the effective operating bandwidth, unlike the classic DVA use one vibration mode only. It means that they can attenuate vibrations at lower and higher excitation frequencies around resonance. This work presents a comparative study on the dynamic behavior for these types of passive high-performance DVAs. To study the dynamic behavior for the types of proposed DVAs, two different excitation sources were proposed which are the following; the first one is the random ground motion excitation; and the second is random force excitation. Indeed, for the random ground motion excitation case, the optimal parameters for majority of these device have not been reported before, and therefore in this work were computed. For random force excitation, some numerical solutions for the optimal design of these devices were only determined in this paper because the other one were provided in previous researches. For both random excitation cases, closed-form solutions for dimensionless variances of frequency response of the undamped primary structure for each device were obtained. Then for the minimization for variances, nonlinear unconstrained optimization problems were formulated in order to compute the optimum parameters for each device. The optimality of these solutions was confirmed by the eigenvalues computed from the Hessian matrix. For random ground motion excitation case, the numerical simulations revealed that the DVAs arranged in series, IDVA-C6, and the IDVA-C3 present major effectiveness for suppressing vibration than the other devices (DVAs connected in parallel, 2dof-TVA, and IDVA-C4) and yield more than 13% improvement with respect to the classic DVA, see Fig. 3.9(a). In fact, the relative dynamic performance (RPD) between the high-performance devices (DVAs connected in series, IDVA-C6, and IDVA-C3) and DVAs arranged in parallel, 2dof-TVA, and IDVA-C4 is approximately 2–7% improvement for mass ratio range $0.01 \leq \beta \leq 0.1$. This range was selected because in practical application the maximum value of mass ration is 10%. Additionally, for random force excitation case, these passive high-performance devices can achieve more than 10% improvement with respect to the traditional DVA, see Fig. 3.9(b). In addition, it was found that the dynamic performance both the DVAs arranged in series and IDVA-C6 are exactly equal, see Fig. 3.7(a) and (b). It means that in some practical applications such as the machining process, the DVAs connected in series could be more feasible to implement than IDVA-C6 because the mounting space of the DVA is quite reduced. Although the IDVA-C6 has the advantage for yielding high apparent mass or inertance without modifying the physical size of inerter, the DVAs connected in series and 2dof TVA could be more appropriate for mitigating vibration in applications such as milling process in which mounting space is quite small.

Additionally, the suppression band index (SB) was computed for all devices. It was noted that DVAs connected in series, IDVA-C6, IDVA-C3, and 2dof-TVA can provide more than 30% of widening of SB with respect to the classic DVA. It means that these devices are more effective and robust for mitigating vibration around resonance than the classic DVA.

The numerical solutions for a mass ration $\beta = 10\%$ obtained from H_∞ optimization showed that the performance both the DVAs arranged in series and IDVA-C3 are equal, see Table 4.1. In addition, the frequency response both the DVAs arranged in series and IDVA-C6 are quite similar, see Fig. 4.1. Indeed, it was noted from H_2 optimization that the vibration amplitudes are the same at whole excitation range. In the literature, the IDVA-C6 is well known as the rotational inertial double tuned mass damper. It is very interesting that the rotational inertial double tuned mass damper can be replaced by DVAs arranged in series since these devices have the same dynamic performance.

The concept of equivalent mass ratio was introduced in order to demonstrate that these devices are better than the classic DVA. Indeed, for a mass ratio $\beta = 0.1$, the physical mass of classic DVA need to be increased by approximately 66.2% to yield the same performance than the IDVA-C6 or DVAs arranged in series.

Although the random excitation sources studied in this paper are not sufficient to demonstrate that these devices are better under the effect of transient and earthquakes loads than other reported in the literature, this paper provide guidelines for optimal design under random acceleration excitation for three types of Dynamic Vibration Absorbers. Future works will be focused for the analysis of transient loads in order to evaluate the robustness under uncertainty, especially for the IDVA-C6, DVAs arranged in series and 2dof-TVA.

Acknowledgment

Funding provided by CONACYT through the PhD scholarship number 448057.

Appendix A. Dimensionless functions A_i, B_i, C_i, and D_i

$$A_1(\beta_1, \mu, q, \eta, \zeta_1, \zeta_2, \Omega) = -(1+\mu)\Omega^4 + ((1+(\beta_1+1)\mu)\eta^2 + 4\zeta_1\zeta_2(\beta_1+1)(1+\mu)\eta + \mu + \beta_1 + 1)q^2\Omega^2 - \eta^2(\beta_1+1)(1+\mu)q^4$$

$$B_1(\beta_1, \mu, q, \eta, \zeta_1, \zeta_2, \Omega) = -2q\Omega((\beta_1+1)(1+\mu)\zeta_1\eta^2q^2 + ((\beta_1+1)(1+\mu)q^2 - \Omega^2(1+(\beta_1+1)\mu))\eta\zeta_2 - (\mu+\beta_1+1)\Omega^2\zeta_1)$$

$$\begin{aligned} C_1(\beta_1, \mu, q, \eta, \zeta_1, \zeta_2, \Omega) &= -(\mu+1)\Omega^6 + (((1+(\beta_1+1)\mu)\eta^2 + 4\zeta_1\zeta_2(\beta_1+1)(1+\mu)\eta + \mu + \beta_1 + 1)q^2 + 1 + \mu)\Omega^4 - (1+\mu)q^2(\eta^2(\beta_1+1)q^2 + 4\eta\zeta_1\zeta_2 + \eta^2 + 1)\Omega^2 + \eta^2 \\ &\quad q^4(1+\mu) \end{aligned}$$

$$\begin{aligned} D_1(\beta_1, \mu, q, \eta, \zeta_1, \zeta_2, \Omega) &= -2q\Omega((-\zeta_2(1+(\beta_1+1)\mu)\eta - \zeta_1(\mu+\beta_1+1))\Omega^4 + (1+\mu)(q^2\zeta_1(\beta_1+1)\eta^2 + \zeta_2((\beta_1+1)q^2+1)\eta + \zeta_1)\Omega^2 - q^2\eta(\eta\zeta_1+\zeta_2)(1+\mu)) \end{aligned}$$

$$A_2(\beta_1, \mu, q, \eta, \Omega) = -(1+\mu)\Omega^4 + ((1+\mu)^2\eta^2 + \mu + \beta_1 + 1)q^2\Omega^2 - \eta^2(\beta_1+1)(1+\mu)q^4$$

$$B_2(\beta_1, \mu, q, \eta, \zeta_2, \Omega) = 2\zeta_2\eta q\Omega(1+\mu)((1+\mu)\Omega^2 - (\beta_1+1)q^2)$$

$$C_2(\beta_1, \mu, q, \eta, \Omega) = -(\mu+1)\Omega^6 + (((1+\mu)^2\eta^2 + \mu + \beta_1 + 1)q^2 + 1 + \mu)\Omega^4 - (1+\mu)(\eta^2(\beta_1+1)q^2 + 1 + (1+\mu)\eta^2)q^2\Omega^2 + \eta^2q^4(1+\mu)$$

$$D_2(\beta_1, \mu, q, \eta, \zeta_2, \Omega) = 2\zeta_2\eta q\Omega(1+\mu)((1+\mu)\Omega^4 - ((\beta_1+1)q^2 + 1 + \mu)\Omega^2 + q^2)$$

$$A_3(\beta, \alpha, q, \eta, \Omega) = -\Omega^4 + (\eta^2+1)(\beta+\alpha+1)q^2\Omega^2 - 4(1+\beta)\alpha\eta^2q^4$$

$$B_3(\beta, \alpha, q, \eta, \zeta_1, \Omega) = 2q\zeta_1\Omega((\beta+\alpha+1)\Omega^2 - 4q^2\eta^2\alpha(1+\beta))$$

$$C_3(\beta, \alpha, q, \eta, \Omega) = -\Omega^6 + (1 + q^2(\eta^2 + 1)(\beta + \alpha + 1))\Omega^4 - (4\alpha q^2\eta^2(1 + \beta) + (\eta^2 + 1)(\alpha + 1))q^2\Omega^2 + 4\alpha\eta^2q^4$$

$$D_3(\beta, \alpha, q, \eta, \zeta_1, \Omega) = 2q\zeta_1\Omega((\beta + \alpha + 1)\Omega^4 - (1 + (1 + 4q^2\eta^2(1 + \beta))\alpha)\Omega^2 + 4\alpha\eta^2q^2)$$

$$A_4(\beta, \mu, q, \eta, \Omega) = -\mu\Omega^4 + ((1 + (1 + \beta)\mu)\eta^2 + 1 + \beta)\mu q^2\Omega^2 - (1 + \beta)\mu\eta^2q^4$$

$$B_4(\beta, \mu, q, \eta, \zeta_1, \Omega) = 2\zeta_1\Omega q(\Omega^2 - (1 + \beta)(\mu\eta^2 + 1)q^2)$$

$$C_4(\beta, \mu, q, \eta, \Omega) = -\mu\Omega^6 + (1 + ((1 + (1 + \beta)\mu)\eta^2 + 1 + \beta)q^2)\mu\Omega^4 - q^2(1 + ((1 + \beta)q^2 + \mu + 1)\eta^2)\mu\Omega^2 + \mu\eta^2q^4$$

$$D_4(\beta, \mu, q, \eta, \zeta_1, \Omega) = 2\zeta_1\Omega q(\Omega^4 - (1 + (1 + \beta)(\mu\eta^2 + 1)q^2)\Omega^2 + q^2(\mu\eta^2 + 1))$$

$$A_5(\beta, \mu, q, \eta, \Omega) = -\mu\Omega^4 + ((1 + (\beta + 1)\mu)\eta^2 + \beta + 1)\mu q^2\Omega^2 - (\beta + 1)\mu\eta^2q^4$$

$$B_5(\beta, \mu, q, \eta, \zeta_1, \Omega) = 2q\zeta_1\Omega((\mu\beta + \mu + 1)\Omega^2 - q^2(\beta + 1))$$

$$C_5(\beta, \mu, q, \eta, \Omega) = -\mu\Omega^6 + (1 + ((1 + (\beta + 1)\mu)\eta^2 + \beta + 1)q^2)\mu\Omega^4 - (1 + (q^2(\beta + 1) + \mu + 1)\eta^2)\mu q^2\Omega^2 + \mu\eta^2q^4$$

$$D_5(\beta, \mu, q, \eta, \zeta_1, \Omega) = 2q\zeta_1\Omega((1 + (\beta + 1)\mu)\Omega^4 - (q^2(\beta + 1) + \mu + 1)\Omega^2 + q^2)$$

$$A_6(\beta, \mu, q, \eta, \zeta_1, \Omega) = 2\zeta_1(-\Omega^4 + ((\mu\beta + \mu + 1)\eta^2 + \beta + 1)q^2\Omega^2 - (1 + \beta)\eta^2q^4)$$

$$B_6(\beta, \mu, q, \eta, \Omega) = \mu q\eta^2\Omega(\Omega^2 - (1 + \beta)q^2)$$

$$C_6(\beta, \mu, q, \eta, \zeta_1, \Omega) = 2\zeta_1(-\Omega^6 + (1 + ((\mu\beta + \mu + 1)\eta^2 + \beta + 1)q^2)\Omega^4 - (1 + ((1 + \beta)q^2 + \mu + 1)\eta^2)q^2\Omega^2 + \eta^2q^4)$$

$$D_6(\beta, \mu, q, \eta, \Omega) = \mu q\eta^2\Omega(\Omega^4 - (1 + (1 + \beta)q^2)\Omega^2 + q^2)$$

$$A_{11}(\mu, q, \eta, \zeta_1, \zeta_2, \Omega) = (\Omega^4 - (4\eta\zeta_1\zeta_2 + \eta^2 + 1)q^2\Omega^2 + \eta^2q^4)(\mu + 1)$$

$$B_{11}(\mu, q, \eta, \zeta_1, \zeta_2, \Omega) = 2q\Omega(1 + \mu)(-(\eta\zeta_2 + \zeta_1)\Omega^2 + \eta q^2(\eta\zeta_1 + \zeta_2))$$

$$A_{22}(\mu, q, \eta, \Omega) = (1 + \mu)(\Omega^4 - (1 + (1 + \mu)\eta^2)q^2\Omega^2 + \eta^2q^4)$$

$$B_{22}(\mu, q, \eta, \zeta_2, \Omega) = 2\zeta_2\eta q\Omega(1 + \mu)(-(1 + \mu)\Omega^2 + q^2)$$

$$A_{33}(\alpha, q, \eta, \Omega) = \Omega^4 - (\eta^2 + 1)(\alpha + 1)q^2\Omega^2 + 4\alpha\eta^2q^4$$

$$B_{33}(\alpha, q, \eta, \zeta_1, \Omega) = 2q\zeta_1\Omega(-(\alpha + 1)\Omega^2 + 4\alpha\eta^2q^2)$$

$$A_{44}(\mu, q, \eta, \Omega) = \mu\Omega^4 - (1 + (\mu + 1)\eta^2)\mu q^2\Omega^2 + \mu\eta^2q^4$$

$$B_{44}(\mu, q, \eta, \zeta_1, \Omega) = 2q\zeta_1\Omega(\mu\eta^2q^2 - \Omega^2 + q^2)$$

$$A_{55}(\mu, q, \eta, \Omega) = \mu\eta^2q^4 + \mu\Omega^4 - (1 + (\mu + 1)\eta^2)\mu q^2\Omega^2$$

$$B_{55}(\mu, q, \zeta_1, \Omega) = 2q\zeta_1\Omega(-(\mu + 1)\Omega^2 + q^2)$$

$$A_{66}(\mu, q, \eta, \zeta_1, \Omega) = 2\zeta_1(\Omega^4 - q^2(1 + (\mu + 1)\eta^2)\Omega^2 + \eta^2q^4)$$

$$B_{66}(\mu, q, \eta, \Omega) = \mu q\eta^2\Omega(-\Omega^2 + q^2)$$

Appendix B. Optimal curves of μ_{opt}, $\frac{1}{\sqrt{\alpha_{opt}}} = \frac{\rho}{d}$, q_{opt}, η_{opt}, $\zeta_{1,opt}$, and $\zeta_{2,opt}$ for both random excitation cases

(a) Optimal parameters for the random ground motion excitation case (Fig. 8.1)
(b) Optimal parameters for the random force excitation case (Fig. 8.2)
(c) Eigenvalues for both random excitation cases (Figs. 8.3–8.5)

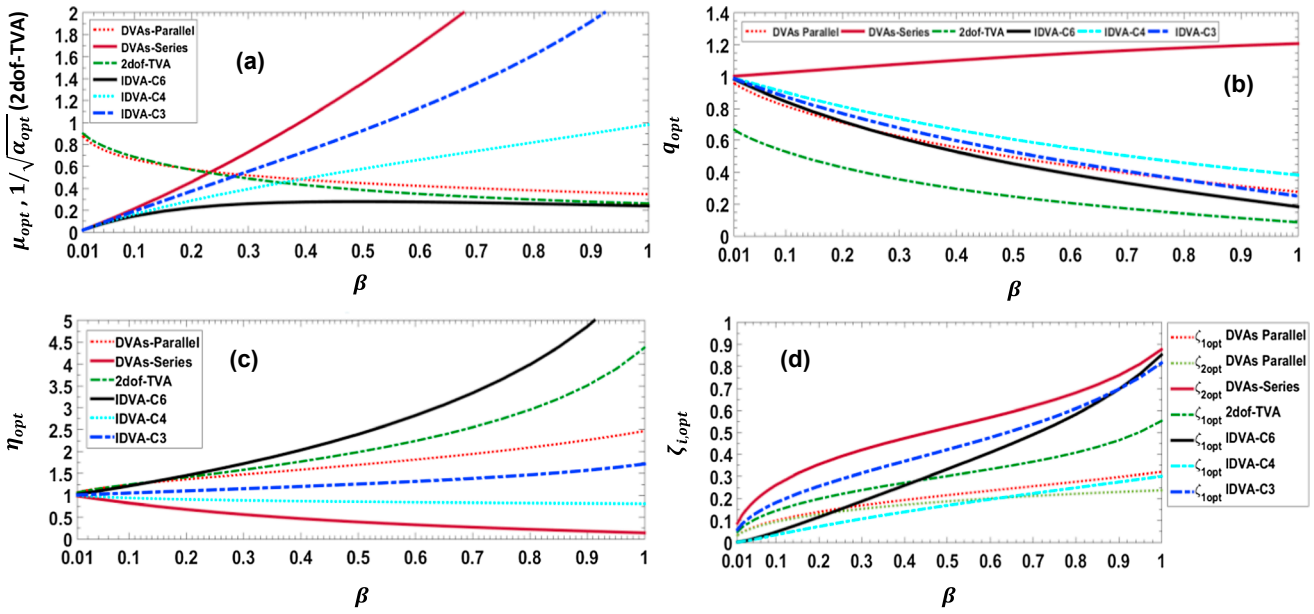

Fig. 8.1. Optimal parameter curves for all devices.

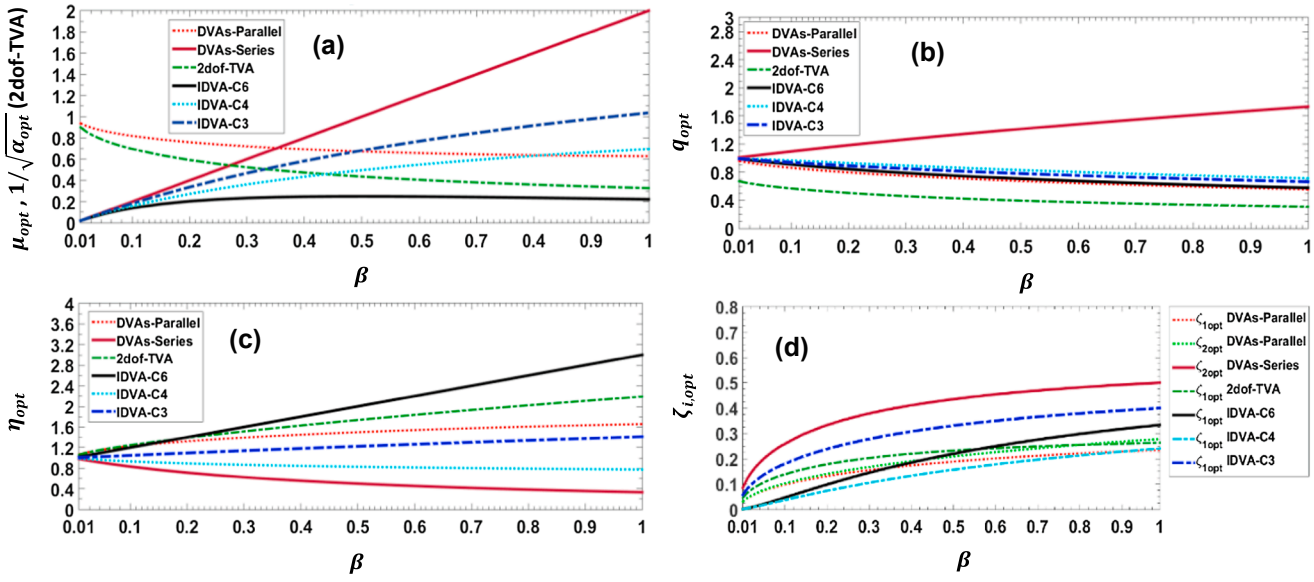

Fig. 8.2. Optimal parameter curves for all devices.

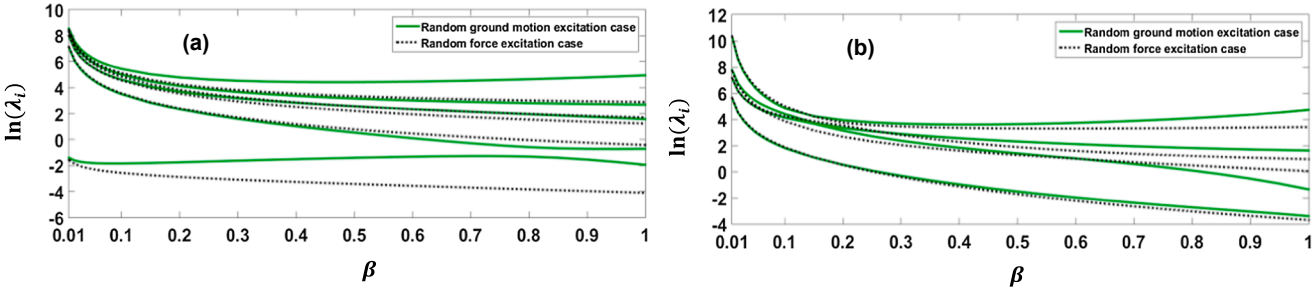

Fig. 8.3. Eigenvalues evaluated at optimal parameters μ_{opt}, q_{opt}, η_{opt}, $\zeta_{1,opt}$, and $\zeta_{2,opt}$: (a) DVAs arranged in parallel; (b) DVAs arranged in series.

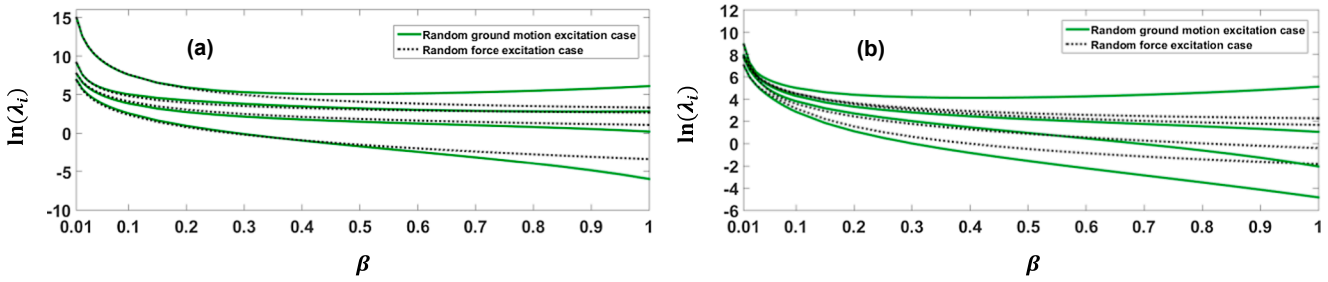

Fig. 8.4. Eigenvalues evaluated at optimal parameters μ_{opt}, q_{opt}, η_{opt}, $\zeta_{1,opt}$: (a) IDVA-C6; (b) IDVA-C3.

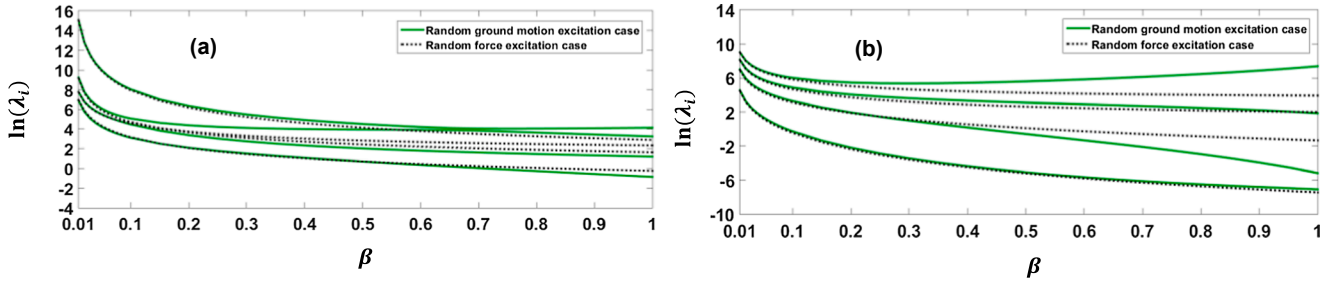

Fig. 8.5. Eigenvalues evaluated at optimal parameters μ_{opt}, q_{opt}, η_{opt}, $\zeta_{1,opt}$: (a) IDVA-C4; (b) 2dof TVA with translational and rotational motion.

Appendix C. Dimensionless functions F_i, G_j, f_i, and g_j

$$f_1(\mu,\beta_1,q,\zeta_1,\zeta_2) = ((\beta_1+1)^3(1+\mu)^2 4q^2\zeta_1^2 + (\beta_1+1)^4(1+\mu)^2q^4 - (1+\mu)((\beta_1+1)2\mu - \beta_1 + 2)(\beta+1)^2q^2 + ((\beta_1+1)\mu+1)^2)((\beta_1+1)\mu+1)^2\zeta_1\zeta_2q^4$$

$$f_2(\mu,\beta_1,q,\zeta_1,\zeta_2) = (4q^2(\beta_1+1)^3(1+\mu)^2\zeta_1^2 + ,\cdots,+((\beta_1+1)\mu+1)^2)\zeta_1^2q^4((4((\beta_1+1)\mu+1))(1+\mu)(\beta_1+1)\zeta_2^2 + \mu\beta_1^2)$$

$$f_3(\mu,\beta_1,q,\zeta_1,\zeta_2) = (4(4q^4(\beta_1+1)^4(1+\mu)^3(\mu+\beta_1+1)\zeta_1^4 + ,\cdots,+0.25((\beta_1+1)\mu+1)^2(1+\mu)(-2+(\beta_1-2)\mu)))\zeta_1\zeta_2q^2$$

$$\begin{aligned} f_4(\mu,\beta_1,q,\zeta_1,\zeta_2) &= (4((4(1+\mu))q^2(\beta_1+1)((4((\beta_1+1)\mu+1))(1+\mu)^2(\beta_1+1)^2\zeta_2^4 + ((\beta_1+1)^2(1+\mu)(\mu+\beta_1+1)q^2 + (\beta_1^2-\beta_1-2)\mu^2 + (-\beta_1^2-2\beta_1-4)\mu \\ &\quad + \beta_1^2-\beta_1-2)(1+\mu)(\beta_1+1)\zeta_2^2 + 0.5\mu^2\beta_1^3) + ,\cdots,+0.25\beta_1^2\mu\zeta_2^2((\beta_1+1)^4(1+\mu)^2q^6 + 3\beta_1(\beta_1+1)^2(1+\mu)q^4 + 2\beta_1((\beta_1+1)\mu+1.5\beta_1+1)q^2 \\ &\quad + (1+\mu)\beta_1)))q^2 \end{aligned}$$

$$\begin{aligned} f_5(\mu,\beta_1,q,\zeta_1,\zeta_2) &= \zeta_1(64(1+\mu)^2q^4(\mu+\beta_1+1)(\beta_1+1)^2((\beta_1+1)(1+\mu)\zeta_2^2 + (0.25\beta_1-0.25)\mu - 0.5\beta_1 - 0.5)\zeta_1^4 + , \\ &\quad \cdots,+(16((\beta_1+1)\mu+1)) - (2((\beta_1^3-2\beta_1-1)\mu^3 + (-3-3.5\beta_1)\mu^2 + (-\beta_1-3)\mu - 0.5\beta_1^3 + 0.5\beta_1 - 1))(1+\mu)q^2 + (1+\mu)^4)\zeta_2 \end{aligned}$$

$$\begin{aligned} f_6(\mu,\beta_1,q,\zeta_1,\zeta_2) &= (64(q^2(1+\mu)^2(\beta_1+1)^3(\mu+\beta_1+1)\zeta_2^4 + ,\cdots,+0.0625\mu^2\beta_1^3))(1+\mu)q^2\zeta_1^4 + , \\ &\quad \cdots,+(0.25(1+\mu))((\beta_1-2)\mu - 2\beta_1 - 2)(\beta_1+1)^2q^4 - 0.5\beta_1((\beta_1+2)\mu + 2\beta_1 + 2)q^2 - (0.5(1+\mu))\beta_1)\mu\zeta_2^2 \end{aligned}$$

$$\begin{aligned} f_7(\mu,\beta_1,q,\zeta_1,\zeta_2) &= 4\zeta_1((4(1+\mu))q^2(\mu+\beta_1+1)^3\zeta_1^4 + ,\cdots,+(0.25((\beta_1^3-\beta_1+2)\mu^3 + (2\beta_1+6)\mu^2 + (7\beta_1+6)\mu - 2\beta_1^3 + 4\beta_1 + 2))(1+\mu)q^2 - 0.5(1+\mu)^4)\zeta_2 \end{aligned}$$

$$f_8(\mu,\beta_1,q,\zeta_1,\zeta_2) = 16q^2\zeta_2^2(1+\mu)(\mu+\beta_1+1)^3\zeta_1^4 + ,\cdots,+\beta_1^2((\mu+\beta_1+1)^2q^2 + (1+\mu)\beta_1)\mu q^2\zeta_2^2$$

$$f_9(\mu,\beta_1,q,\zeta_1,\zeta_2) = \zeta_1\zeta_2((4(1+\mu))q^2(\mu+\beta_1+1)^3\zeta_1^2 + (\mu+\beta_1+1)^4q^4 - (2(1+\mu-0.5\beta_1))(1+\mu)(\mu+\beta_1+1)^2q^2 + (1+\mu)^4)$$

$$f_{10}(\mu,\beta_1,q,\zeta_1,\zeta_2) = ((\beta_1+1)^4q^4 + (\beta_1-2)(\beta_1+1)^2(\mu+1)q^2 + (\mu+1)^2)q^4(\mu+1)^2$$

$$\begin{aligned} f_{11}(\mu,\beta_1,q,\zeta_1,\zeta_2) &= (4(((\beta_1+1)^2(((\beta_1+1)\zeta_2^2 + 0.25\beta_1 - 0.5)\mu + (\beta_1+1)(\zeta_2^2-0.5))q^4 - (2((-0.25 + (\beta_1+1)\zeta_2^2)\mu + (\beta_1+1)(\zeta_2^2-0.5)))(\mu+1)q^2 \\ &\quad + (\mu+1)^2(\mu\zeta_2^2 + \zeta_2^2 - 0.5)))q^2(\mu+1) \end{aligned}$$

$$f_{12}(\mu,\beta_1,q,\zeta_1,\zeta_2) = (\mu+\beta_1+1)^2q^4 - (2(\mu+0.5\beta_1+1))(\mu+1)q^2 + (\mu+1)^2$$

$$f_{13}(\beta, \alpha, q, \zeta_1) = 16q^4((0.0625 + (1+\beta)^4q^4 + 4(1+\beta)^2((\zeta_1^2 + 0.0625)\beta + \zeta_1^2 - 0.125)q^2)\alpha^2 - (0.5(0.5 + (1+\beta)q))(1+\beta)(-0.5 + (1+\beta)q)\alpha + 0.0625(1+\beta)^2)(\beta - \alpha + 1)^2$$

$$f_{14}(\beta, \alpha, q, \zeta_1) = 20q^2(((-0.2\beta + 0.4)\alpha^2 + (\beta^2 + \beta)\alpha - 0.4(1+\beta)^2)(1+\beta)^2\alpha q^4 + ,\cdots, +0.1\alpha^2 + 0.05\alpha\beta + (0.05(1+\beta))(\beta - 2))(\beta - \alpha + 1)$$

$$f_{15}(\beta, \alpha, q, \zeta_1) = (\alpha^4 + (-4\beta^3 + 4\beta)\alpha^3 + (8\beta^4 + 16\beta^3 + 6\beta^2 - 4\beta - 2)\alpha^2 - 4\beta(1+\beta)^3\alpha + (1+\beta)^4)q^4 + (4\alpha^4\zeta_1^2 + (12\beta\zeta_1^2 - 2)\alpha^3 + ((16\zeta_1^2 + 1)\beta^3 + 12\beta^2\zeta_1^2 + (-12\zeta_1^2 - 3)\beta - 8\zeta_1^2 + 2)\alpha^2 + (-12\beta^3\zeta_1^2 - 24\beta^2\zeta_1^2 - 4\beta^3 - 12\beta\zeta_1^2 + 6\beta + 2)\alpha + (4((\zeta_1^2 + 0.25)\beta + \zeta_1^2 - 0.5))(1+\beta)^2)q^2 + (-1+\alpha)^2$$

$$f_{16}(\beta, \alpha, q) = q^2\beta^3\alpha^2$$

$$f_{17}(\mu, \beta, q, \zeta_1) = ((1+\beta)^4q^4 - 2(1+\beta)^2((-2\zeta_1^2 + \mu - 0.5)\beta - 2\zeta_1^2 + \mu + 1)q^2 + (\mu\beta + \mu + 1)^2)q^4\mu^2$$

$$f_{18}(\mu, \beta, q, \zeta_1) = -(2((1+\beta)^3(-4\zeta_1^2 + \mu)q^4 - (1+\beta)((1+\beta)\mu^2 + 2\mu - 4\zeta_1^2)q^2 + (0.5\beta + 1)\mu^2 + \mu))q^2\mu$$

$$f_{19}(\mu, \beta, q, \zeta_1) = 4\zeta_1^2(1+\beta)^3q^6 + (-8\zeta_1^2 + (1+\beta)\mu^2)(1+\beta)q^4 + (4\zeta_1^2 - \mu^2(\beta+2))q^2 + \mu^2$$

$$f_{20}(\mu, \beta, q, \zeta_1) = ((\beta+1)^6q^6 - 2(\beta+1)^4((\mu - 1.5)\beta + \mu + 1)q^4 + (\beta+1)^2((\mu^2 - 2\mu + 3)\beta^2 + (2\mu^2 - 2)\beta + (\mu+1)^2)q^2 + \beta^3)q^2\mu^2$$

$$f_{21}(\mu, \beta, q, \zeta_1) = -(2((\beta+1)^4q^4 - (\beta+1)^2((\mu-2)\beta + \mu + 2)q^2 + (-0.5\mu + 1)\beta^2 + (0.5\mu - 1)\beta + \mu + 1))(\beta+1)q^2\mu^2$$

$$f_{22}(\mu, \beta, q, \zeta_1) = 4\zeta_1^2(\beta+1)^5q^6 + (((-8\mu + 8)\beta - 8\mu - 8)\zeta_1^2 + \mu^2(\beta+1))(\beta+1)^3q^4 + (4(((\mu^2 - \mu + 1)\beta^2 + (2\mu^2 + \mu - 1)\beta + (\mu+1)^2)\zeta_1^2 + 0.25\mu^2(\beta+1)(\beta-2)))(\beta+1)q^2 + \mu^2$$

$$f_{23}(\mu, \beta, q, \zeta_1) = (4(\zeta_1^2(1+\beta)^5q^6 + 0.25(1+\beta)^3(((-8\mu+8)\beta - 8\mu - 8)\zeta_1^2 + \mu^2(1+\beta))q^4 + (1+\beta)(((\mu^2 - \mu + 1)\beta^2 + (2\mu^2 + \mu - 1)\beta + (\mu+1)^2)\zeta_1^2 + 0.25\mu^2(1+\beta)(\beta-2))q^2 + 0.25\mu^2))q^2$$

$$f_{24}(\mu, \beta, q, \zeta_1) = -8\zeta_1^2((1+\beta)^4q^4 - (1+\beta)^2((\mu-1)\beta + \mu + 2)q^2 + \beta\mu + \mu + 1)q^2$$

$$f_{25}(\mu, \beta, q, \zeta_1) = 4\zeta_1^2(1 + (1+\beta)^3q^4 + (-2\beta - 2)q^2)$$

$$g_1(\mu, \beta_1, q, \zeta_1, \zeta_2) = 4\beta_1(1+\mu)q^5((\beta_1+1)\mu + 1)^2\zeta_1^2\zeta_2$$

$$g_2(\mu, \beta_1, q, \zeta_1, \zeta_2) = 4\beta_1(1+\mu)q^5\zeta_1^3((4((\beta_1+1)\mu + 1))(1+\mu)(\beta_1+1)\zeta_2^2 + \mu\beta_1^2)$$

$$g_3(\mu, \beta_1, q, \zeta_1, \zeta_2) = 16\beta_1(1+\mu)^2q^3\zeta_1^2((\beta_1+1)(\mu + \beta_1 + 1)q^2\zeta_1^2 + (((\beta_1+1)\mu + 1)\zeta_2^2 - 0.5\mu - 0.5)(1 + (\beta_1+1)q^2))\zeta_2$$

$$g_4(\mu, \beta_1, q, \zeta_1, \zeta_2) = 4\beta_1(1+\mu)q((4(1+\mu))q^2((4 + (4\beta_1+4)\mu)\zeta_2^2\beta_1 + 1)(\mu + \beta_1 + 1)q^2 + (\beta_1+1)\mu^2 + (-2\beta_1 - 1)\mu + \beta_1 - 2)\zeta_1^2 + \mu(((\beta_1+1)^2\mu^2 + (2\beta_1+2)\mu + \beta_1^2 + 1)q^4 + ((-2\beta_1 - 2)\mu^2 - 4\mu + 2\beta_1 - 2)q^2 + (1+\mu)^2))\zeta_1\zeta_2^2$$

$$g_5(\mu, \beta_1, q, \zeta_1, \zeta_2) = 16\beta_1(1+\mu)q\zeta_1^2((4(((\beta_1+1)\mu^2 + 2\mu + \beta_1 + 1)\zeta_2^2 + (0.25\beta_1 - 0.5)\mu - 0.5\beta_1 - 0.5))(1+\mu)q^2\zeta_1^2 + (4((\beta_1+1)\mu + 1))(1+\mu)q^2\zeta_2^4 + ,\cdots, +((-0.5\beta_1 + 1)\mu^2 + 2\mu + 0.5\beta_1 + 1)q^2 + 0.25(1+\mu)^2)\zeta_2$$

$$g_6(\mu, \beta_1, q, \zeta_1, \zeta_2) = 16\beta_1(1+\mu)^2q(4q^2\mu(\mu + \beta_1 + 1)\zeta_1^4 + ,\cdots, +((((\beta_1+1)\mu + 1)q^4(\beta_1+1) + ((-2\beta_1 - 2)\mu + \beta_1 - 2)q^2 + 1 + \mu)\zeta_2^2 - (0.5(\beta_1+1))(1+\mu)q^4 + ((0.5\beta_1 + 1)\mu - 0.5\beta_1 + 1)q^2 - 0.5\mu - 0.5)\mu)\zeta_1\zeta_2^2$$

$$g_7(\mu, \beta_1, q, \zeta_1, \zeta_2) = 16\beta_1(1+\mu)q((4(1+\mu))(q^2\mu(\mu + \beta_1 + 1)\zeta_2^2 + 0.25 + 0.25\mu)\zeta_1^4 + ,\cdots, +0.25\beta_1^2\mu^2q^4\zeta_2^2)\zeta_2$$

$$g_8(\mu, \beta_1, q, \zeta_1, \zeta_2) = 4\beta_1(1+\mu)q((4(1+\mu))(q^2\mu(\mu + \beta_1 + 1) + 1 + \mu)\zeta_1^2 + \mu((\mu + \beta_1 + 1)^2q^4 - 2(1+\mu)^2q^2 + (1+\mu)^2))\zeta_1\zeta_2^2$$

$$g_9(\mu, \beta_1, q, \zeta_1, \zeta_2) = 4\beta_1(1+\mu)^3q\zeta_1^2\zeta_2$$

$$F_1(\mu, \beta_1, q, \zeta_1, \zeta_2) = (4(1+\mu))\zeta_2((\beta_1+1)\mu + 1)^2q^6(\beta_1+1)\zeta_1^3 + ((\beta_1+1)\mu + 1)^2q^4(q^4(\beta_1+1)^2(1+\mu) + ((-2\beta_1 - 2)\mu - \beta_1 - 2)q^2 + 1 + \mu)\zeta_2\zeta_1$$

$$F_2(\mu, \beta_1, q, \zeta_1, \zeta_2)$$
$$= (16(((\beta_1 + 1)\mu + 1)(1 + \mu)q^4(\beta_1 + 1)^2\zeta_2^2 + 0.25q^4\mu\beta_1^2(\beta_1 + 1)))(1 + \mu)q^2$$
$$\zeta_1^4 + (4((1 + \mu)((\beta_1 + 1)\mu + 1)q^4(q^4(\beta_1 + 1)^2(1 + \mu) + ((-2\beta_1 - 2)\mu - \beta_1 - 2)q^2 + 1 + \mu)(\beta_1 + 1)\zeta_2^2 + 0.25\beta_1^2$$
$$(q^4(\beta_1 + 1)^2(1 + \mu) + ((-2\beta_1 - 2)\mu - \beta_1 - 2)q^2 + 1 + \mu)q^4\mu))\zeta_1^2$$

$$F_3(\mu, \beta_1, q, \zeta_1, \zeta_2)$$
$$= 16q^6(1 + \mu)^2(\mu + \beta_1 + 1)(\beta_1 + 1)^2\zeta_2\zeta_1^5 + ,$$
$$\cdots, +((4(1 + \mu))((\beta_1 + 1)\mu + 1)q^2(q^4(\beta_1 + 1)^2(1 + \mu) + ((-2\beta_1 - 2)\mu - \beta_1 - 2)q^2 + 1 + \mu)(1 + (\beta_1 + 1)q^2)$$
$$\zeta_2^2 - (2((\beta_1 + 1)^3(1 + \mu)^3q^6 - (0.5((\beta_1 + 1)\mu + 1))((\beta_1^2 + 3\beta_1 + 2)\mu^2 + (5\beta_1 + 4)\mu + 2\beta_1 + 2)q^4 - ((\beta_1 + 1)\mu + 1)(1 + \mu)^2q^2$$
$$+ 0.5(1 + \mu)^2(2 + (\beta_1 + 2)\mu)))q^2)\zeta_2\zeta_1$$

$$F_4(\mu, \beta_1, q, \zeta_1, \zeta_2)$$
$$= (16((4((\beta_1 + 1)\mu + 1))(1 + \mu)q^2(\beta_1 + 1)\zeta_2^4 + q^2((\beta_1 + 1)^2(1 + \mu)(\mu + \beta_1 + 1)q^2 + (-\beta_1^2 - 3\beta_1 - 2)\mu^2 - (\beta_1 + 2)^2\mu + \beta_1^2 - \beta_1 - 2)\zeta_2^2))(1 + \mu)q^2$$
$$\zeta_1^4 + , \cdots, +\beta_1^2q^6((\beta_1 + 1)^2(1 + \mu)q^2 + \beta_1)\mu\zeta_2^2$$

$$F_5(\mu, \beta_1, q, \zeta_1, \zeta_2) = 16q^2(1 + \mu)(\mu + \beta_1 + 1)((4(\beta_1 + 1))q^2(1 + \mu)\zeta_2^2 - ((\beta_1 + 2)\mu + 2\beta_1 + 2)q^2)\zeta_2$$
$$\zeta_1^5 + (4(1 + \mu))\zeta_2((16((\beta_1 + 1)\mu + 1))(1 + \mu)q^4(\beta_1 + 1)\zeta_2^4 + , \cdots, +(2(\mu + 0.5\beta_1 + 1))(1 + \mu)^2q^2 + (1 + \mu)^3)\zeta_2\zeta_1$$

$$F_6(\mu, \beta_1, q, \zeta_1, \zeta_2) = (16(4q^2(1 + \mu)(\mu + \beta_1 + 1)(\beta_1 + 1)\zeta_2^4 + (-((\beta_1 + 2)\mu + 2\beta_1 + 2)(\mu + \beta_1 + 1)q^2 + (1 + \mu)^2(\beta_1 + 1))\zeta_2^2))(1 + \mu)q^2\zeta_1^4 + ,$$
$$\cdots, +\beta_1^2q^4((4(\beta_1 + 1))q^2(1 + \mu)\zeta_2^2 - ((\beta_1 + 2)\mu + 2\beta_1 + 2)q^2)\mu\zeta_2^2$$

$$F_7(\mu, \beta_1, q, \zeta_1, \zeta_2)$$
$$= 16q^2(1 + \mu)^2(\mu + \beta_1 + 1)\zeta_2\zeta_1^5 + ,$$
$$\cdots, +((4(1 + \mu))((\beta_1 + 1)(\mu + \beta_1 + 1)^2q^6 + ((\beta_1 - 1)\mu - 1)(1 + \mu)(\beta_1 + 1)q^4 - ((\beta_1 + 1)\mu + 1)(1 + \mu)q^2 + (1 + \mu)^2)\zeta_2^2 -$$
$$(((\beta_1 + 2)\mu + 2\beta_1 + 2)(\mu + \beta_1 + 1)q^4 - (1 + \mu)((4 + \beta_1)\mu + 2\beta_1 + 4)q^2 + 2(1 + \mu)^2)((\mu + \beta_1 + 1)q^2 + 1 + \mu))\zeta_2\zeta_1$$

$$F_8(\mu, \beta_1, q, \zeta_1, \zeta_2) = 16(1 + \mu)^2(\mu + \beta_1 + 1)\zeta_2^2q^2\zeta_1^4 + 4(1 + \mu)^2((\beta_1 + 1)(\mu + \beta_1 + 1)q^4 + ((\beta_1 - 2)\mu - \beta_1 - 2)q^2 + 1 + \mu)\zeta_2^2\zeta_1^2 + \beta_1^2q^4(1 + \mu)\mu\zeta_2^2$$

$$F_9(\mu, \beta_1, q, \zeta_1, \zeta_2) = 4q^2(1 + \mu)^2(\mu + \beta_1 + 1)\zeta_2\zeta_1^3 + (1 + \mu)((\mu + \beta_1 + 1)^2q^4 - (2(\mu + 0.5\beta_1 + 1))(1 + \mu)q^2 + (1 + \mu)^2)\zeta_2\zeta_1$$

$$F_{10}(\mu, \beta_1, q, \zeta_1, \zeta_2) = (\beta_1 + 1)^2(\mu + 1)q^8 - (\mu + 1)^2(\beta_1 + 2)q^6 + (\mu + 1)^3q^4$$

$$F_{11}(\mu, \beta_1, q, \zeta_1, \zeta_2) = -((-4\beta_1\zeta_2^2 - 4\zeta_2^2 + \beta_1 + 2)\mu - 4\beta_1\zeta_2^2 - 4\zeta_2^2 + 2\beta_1 + 2)q^6 + (\mu + 1)(-8\mu\zeta_2^2 - 8\zeta_2^2 + 2\mu + 4)q^4 + 4(\mu + 1)^2(\mu\zeta_2^2 + \zeta_2^2 - 0.5)q^2$$

$$F_{12}(\mu, \beta_1, q, \zeta_1, \zeta_2) = (\mu + 1)q^4 + (-2\mu + \beta_1 - 2)q^2 + \mu + 1$$

$$F_{13}(\alpha, \beta, q, \zeta_1)$$
$$= 16\alpha^2(\beta + 1)^2(\beta - \alpha + 1)^2q^8 + (64((-\beta\zeta_1^2 - \zeta_1^2 + 0.0625\beta + 0.125)\alpha^2 + (\beta + 1)(\beta\zeta_1^2 + \zeta_1^2 - 0.0625\beta)\alpha - 0.125(\beta + 1)^2))\alpha$$
$$(\beta - \alpha + 1)q^6 + (\alpha^4 - 2\beta\alpha^3 + (\beta^2 - 2\beta - 2)\alpha^2 + (2(\beta + 1))\beta\alpha + (\beta + 1)^2)q^4$$

$$F_{14}(\alpha, \beta, q, \zeta_1) = (64((0.0625\beta + 0.125)\alpha^2 + (3/16(\beta + 1))\beta\alpha - 0.125(\beta + 1)^2))\alpha(\beta - \alpha + 1)q^6 + , \cdots, +(3(-2/3\alpha^2 + \beta\alpha + 1/3\beta + 2/3))(-1 + \alpha)q^2$$

$$F_{15}(\alpha, \beta, q, \zeta_1)$$
$$= (\alpha^4 + 2\beta\alpha^3 + (\beta^2 - 2\beta - 2)\alpha^2 - (2(\beta + 1))\beta\alpha + (\beta + 1)^2)$$
$$q^4 + (3(4/3\alpha^3\zeta_1^2 + (4/3\beta\zeta_1^2 + 4/3\zeta_1^2 - 2/3)\alpha^2 + (-4/3\zeta_1^2 - 1/3\beta)\alpha - 4/3\beta\zeta_1^2 - 4/3\zeta_1^2 + 1/3\beta + 2/3))(-1 + \alpha)q^2 + (-1 + \alpha)^2$$

$$F_{16}(\mu, \beta, q, \zeta_1) = \mu^2(1 + \beta)^2q^8 + (-(2(1 + \beta))\mu^3 + (4(\zeta_1^2\beta + \zeta_1^2 - 0.25\beta - 0.5))\mu^2)q^6 + (\mu^4 + 2\mu^3 + \mu^2)q^4$$

$$F_{17}(\mu, \beta, q, \zeta_1) = ((4(-0.5\beta - 0.5))\mu^2 + 8\zeta_1^2(1 + \beta)\mu)q^6 + (-8\zeta_1^2\mu + 2\mu^3 + 4\mu^2)q^4 + ((\beta - 2)\mu^3 - 2\mu^2)q^2$$

$$F_{18}(\mu, \beta, q, \zeta_1) = 4\zeta_1^2(1 + \beta)q^6 + (-8\zeta_1^2 + \mu^2)q^4 + ((\beta - 2)\mu^2 + 4\zeta_1^2)q^2 + \mu^2$$

$$F_{19}(\mu, \beta, q, \zeta_1) = \mu^2(\beta + 1)^4q^8 - (2((\beta + 1)\mu^3 - (0.5(\beta - 2))\mu^2))(\beta + 1)^2q^6 + ((\beta + 1)^2\mu^3 + (2(\beta + 1))\mu^3 + \mu^2)q^4$$

$$F_{20}(\mu, \beta, q, \zeta_1) = (-2\beta - 2)\mu^2(\beta + 1)^2q^6 + (2(\beta + 1)^2\mu^3 + (4\beta + 4)\mu^2)q^4 + (-(\beta + 2)\mu^3 - 2\mu^2)q^2$$

$$F_{21}(\mu, \beta, q, \zeta_1) = 4\zeta_1^2(\beta + 1)^3q^6 + ((\beta + 1)^2\mu^2 - 8\zeta_1^2(\beta + 1)^2\mu - 8\zeta_1^2(\beta + 1))q^4 + ((4\zeta_1^2\beta + 4\zeta_1^2 - \beta - 2)\mu^2 + 4\zeta_1^2(\beta + 2)\mu + 4\zeta_1^2)q^2 + \mu^2$$

$$F_{22}(\mu, \beta, q, \zeta_1) = 4\zeta_1^2(1 + \beta)^3q^8 + ((-8\mu\beta - 8\mu - 8)\zeta_1^2 + \mu^2(1 + \beta))(1 + \beta)q^6 + ((4(\mu + 1))(\mu\beta + \mu + 1)\zeta_1^2 - \mu^2(\beta + 2))q^4 + \mu^2q^2$$

$$F_{23}(\mu, \beta, q, \zeta_1) = -8\zeta_1^2(1 + \beta)^2q^6 + 8\zeta_1^2((\mu + 1)\beta + \mu + 2)q^4 - 8\zeta_1^2(\mu + 1)q^2$$

$$F_{24}(\beta, q, \zeta_1) = 4\zeta_1^2(1+\beta)q^4 - 8\zeta_1^2 q^2 + 4\zeta_1^2$$

$$G_1(\mu, \beta_1, q, \zeta_1, \zeta_2) = \beta_1 q^5((\beta_1+1)\mu+1)^2\zeta_2\zeta_1^2$$

$$G_2(\mu, \beta_1, q, \zeta_1, \zeta_2) = 4\beta_1 q(((\beta_1+1)\mu+1)q^4(\beta_1+1)(1+\mu)\zeta_2^2 + 0.25\beta_1^2 q^4\mu)\zeta_1^3$$

$$G_3(\mu, \beta_1, q, \zeta_1, \zeta_2) = \beta_1 q((4(\beta_1+1))(\mu+\beta_1+1)q^4(1+\mu)\zeta_2\zeta_1^4 + (4(((\beta_1+1)\mu+1)q^2(1+(\beta_1+1)q^2)(1+\mu)\zeta_2^2 - 0.5(1+\mu)^2q^2(1+(\beta_1+1)q^2)))\zeta_2\zeta_1^2)$$

$$G_4(\mu, \beta_1, q, \zeta_1, \zeta_2) = \beta_1 q((4((4((\beta_1+1)\mu+1))(1+\mu)q^2\zeta_2^4 + ((\beta_1+1)(\mu+\beta_1+1)q^2 + (\beta_1+1)\mu^2 + (-2\beta_1-1)\mu+\beta_1-2)q^2(1+\mu)\zeta_2^2))\zeta_1^3 + \mu(((\beta_1+1)^2\mu^2 + (2\beta_1+2)\mu+\beta_1^2+1)q^4 + ((-2\beta_1-2)\mu^2 - 4\mu + 2\beta_1 - 2)q^2 + (1+\mu)^2)\zeta_2^2\zeta_1)$$

$$G_5(\mu, \beta_1, q, \zeta_1, \zeta_2) = \beta_1 q((4(4q^2((\beta_1+1)\mu^2 + 2\mu + \beta_1 + 1)\zeta_2^2 + q^2((\beta_1-2)\mu - 2\beta_1 - 2)))(1+\mu)\zeta_2\zeta_1^4 + (4((4((\beta_1+1)\mu+1))(1+\mu)q^2\zeta_2^4 + ,\cdots, +((-0.5\beta_1+1)\mu^2 + 2\mu + 0.5\beta_1 + 1)q^2 + 0.25(1+\mu)^2))\zeta_2\zeta_1^2)$$

$$G_6(\mu, \beta_1, q, \zeta_1, \zeta_2) = \beta_1 q(16q^2\mu\zeta_2^2(1+\mu)(\mu+\beta_1+1)\zeta_1^5 + ,\cdots, +\mu((4(((\beta_1+1)\mu+1)q^4(\beta_1+1) + ((-2\beta_1-2)\mu+\beta_1-2)q^2+1+\mu))(1+\mu)\zeta_2^2 - (2(1+\mu))((\beta_1+1)(1+\mu)q^4 + ((-\beta_1-2)\mu+\beta_1-2)q^2+1+\mu))\zeta_2^2\zeta_1)$$

$$G_7(\mu, \beta_1, q, \zeta_1, \zeta_2) = \beta_1 q((4(4\mu(\mu+\beta_1+1)q^2\zeta_2^2 + 1 + \mu))(1+\mu)\zeta_2\zeta_1^4 + ,\cdots, +\mu^2 q^4\beta_1^2\zeta_2^3)$$

$$G_8(\mu, \beta_1, q, \zeta_1, \zeta_2) = \beta_1 q((4(\mu(\mu+\beta_1+1)q^2+1+\mu))(1+\mu)\zeta_2^2\zeta_1^3 + \mu((\mu+\beta_1+1)^2q^4 - 2(1+\mu)^2q^2 + (1+\mu)^2)\zeta_2^2\zeta_1)$$

$$G_9(\mu, \beta_1, q, \zeta_1, \zeta_2) = \beta_1 q(1+\mu)^2\zeta_2\zeta_1^2$$

References

[1] Ormondroyd J, Den Hartog JP. The theory of the dynamic vibration absorber. Trans ASME 1928.

[2] Cheung YL, Wong WO. H-infinity optimization of a variant design of the dynamic vibration absorber – revisited and new results. J Sound Vib 2011;330:3901–12. https://doi.org/10.1016/j.jsv.2011.03.027.

[3] Cheung YL, Wong WO. H_2 optimization of a non-traditional dynamic vibration absorber for vibration control of structures under random force excitation. J Sound Vib 2011;330:1039–44. https://doi.org/10.1016/j.jsv.2010.10.031.

[4] Nishihara O. Exact optimization of a three-element dynamic vibration absorber: minimization of the maximum amplitude magnification factor. J Vib Acoust 2018;141. https://doi.org/10.1115/1.4040575. 011001–011001-7.

[5] Anh ND, Nguyen NX, Hoa LT. Design of three-element dynamic vibration absorber for damped linear structures. J Sound Vib 2013;332:4482–95. https://doi.org/10.1016/j.jsv.2013.03.032.

[6] Sinha A. Optimal damped vibration absorber for narrow band random excitations: a mixed H_2/H_∞ optimization. Probabilist Eng Mech 2009;24:251–4. https://doi.org/10.1016/j.probengmech.2008.06.005.

[7] Asami T, Nishihara O, Baz AM. Analytical Solutions to H_∞ and H_2 optimization of dynamic vibration absorbers attached to damped linear systems. J Vib Acoust 2002;124:284. https://doi.org/10.1115/1.1456458.

[8] Tigli OF. Optimum vibration absorber (tuned mass damper) design for linear damped systems subjected to random loads. J Sound Vib 2012;331:3035–49. https://doi.org/10.1016/j.jsv.2012.02.017.

[9] Zilletti M, Elliott SJ, Rustighi E. Optimisation of dynamic vibration absorbers to minimise kinetic energy and maximise internal power dissipation. J Sound Vib 2012;331:4093–100. https://doi.org/10.1016/j.jsv.2012.04.023.

[10] Shum KM. Tuned vibration absorbers with nonlinear viscous damping for damped structures under random load. J Sound Vib 2015;346:70–80. https://doi.org/10.1016/j.jsv.2015.02.003.

[11] Krenk S, Høgsberg J. Tuned mass absorber on a flexible structure. J Sound Vib 2014;333:1577–95. https://doi.org/10.1016/j.jsv.2013.11.029.

[12] Cheung YL, Wong WO, Cheng L. Optimization of a hybrid vibration absorber for vibration control of structures under random force excitation. J Sound Vib 2013;332:494–509. https://doi.org/10.1016/j.jsv.2012.09.014.

[13] Alujević N, Zhao G, Depraetere B, Sas P, Pluymers B, Desmet W. H_2 optimal vibration control using inertial actuators and a comparison with tuned mass dampers. J Sound Vib 2014;333:4073–83. https://doi.org/10.1016/j.jsv.2014.04.038.

[14] Gao P, Xiang C, Liu H, Zhou H. Reducing variable frequency vibrations in a powertrain system with an adaptive tuned vibration absorber group. J Sound Vib 2018;425:82–101. https://doi.org/10.1016/j.jsv.2018.03.034.

[15] Shen Y, Peng H, Li X, Yang S. Analytically optimal parameters of dynamic vibration absorber with negative stiffness. Mech Syst Signal Process 2017;85:193–203. https://doi.org/10.1016/j.ymssp.2016.08.018.

[16] Xiuchang H, Zhiwei S, Hongxing H. Optimal parameters for dynamic vibration absorber with negative stiffness in controlling force transmission to a rigid foundation. Int J Mech Sci 2019;152:88–98. https://doi.org/10.1016/j.ijmecsci.2018.12.033.

[17] Abe M, Fujino Y. Dynamic characterization of multiple tuned mass dampers and some design formulas. Earthq Eng Struct Dyn 1994;23:813–35.

[18] Xu K, Igusa T. Dynamic characteristics of multiple substructures with closely spaced frequencies. Earthq Eng Struct Dyn 1992;21:1059–70. https://doi.org/10.1002/eqe.4290211203.

[19] Yamaguchi H, Harnpornchai N. Fundamental characteristics of Multiple Tuned Mass Dampers for suppressing harmonically forced oscillations. Earthq Eng Struct Dyn 1993;22:51–62. https://doi.org/10.1002/eqe.4290220105.

[20] Joshi AS, Jangid RS. Optimum parameters of multiple tuned mass dampers for base-excited damped systems. J Sound Vib 1997;202:657–67. https://doi.org/10.1006/jsvi.1996.0859.

[21] Li C, Liu Y. Optimum multiple tuned mass dampers for structures under the ground acceleration based on the uniform distribution of system parameters. Earthq Eng Struct Dyn 2003;32:671–90. https://doi.org/10.1002/eqe.239.

[22] Zuo L, Nayfeh SA. Optimization of the individual stiffness and damping parameters in multiple-tuned-mass-damper systems. J Vib Acoust 2005;127:77. https://doi.org/10.1115/1.1855929.

[23] Li HN, Ni XL. Optimization of non-uniformly distributed multiple tuned mass damper. J Sound Vib 2007;308:80–97. https://doi.org/10.1016/j.jsv.2007.07.014.

[24] Yang Y, Muñoa J, Altintas Y. Optimization of multiple tuned mass dampers to suppress machine tool chatter. Int J Mach Tools Manuf 2010;50:834–42. https://doi.org/10.1016/j.ijmachtools.2010.04.011.

[25] Ma J, Sheng M, Guo Z, Qin Q. Dynamic analysis of periodic vibration suppressors with multiple secondary oscillators. J Sound Vib 2018;424:94–111. https://doi.org/10.1016/j.jsv.2018.03.002.

[26] Zuo L, Nayfeh SA. The two-degree-of-freedom tuned-mass damper for suppression of single-mode vibration under random and harmonic excitation. J Vib Acoust 2006;128:56. https://doi.org/10.1115/1.2128639.

[27] Zuo L. Effective and robust vibration control using series multiple tuned-mass dampers. J Vib Acoust 2009;131. https://doi.org/10.1115/1.3085879.

[28] Pai PF, Peng H, Jiang S. Acoustic metamaterial beams based on multi-frequency vibration absorbers. Int J Mech Sci 2014;79:195–205. https://doi.org/10.1016/j.ijmecsci.2013.12.013.

[29] Yang Y, Dai W, Liu Q. Design and implementation of two-degree-of-freedom tuned mass damper in milling vibration mitigation. J Sound Vib 2015;335:78–88. https://doi.org/10.1016/j.jsv.2014.09.032.

[30] Smith MC. Synthesis of mechanical networks: the inerter. IEEE Trans Automat Control 2002;47:1657–62.

[31] Chen MZQ, Papageorgiou C, Scheibe F, Wang F, Smith MC. The missing mechanical circuit element. IEEE Circuits Syst Mag 2009:10–26.

[32] Scheibe F, Smith MC. Analytical solutions for optimal ride comfort and tyre grip for passive vehicle suspensions. Veh Syst Dyn 2009;47:1229–52. https://doi.org/10.

1080/00423110802588323.
[33] Hu Y, Chen MZQ, Shu Z. Passive vehicle suspensions employing inerters with multiple performance requirements. J Sound Vib 2014;333:2212–25. https://doi.org/10.1016/j.jsv.2013.12.016.
[34] Shen Y, Chen L, Yang X, Shi D, Yang J. Improved design of dynamic vibration absorber by using the inerter and its application in vehicle suspension. J Sound Vib 2016;361:148–58. https://doi.org/10.1016/j.jsv.2015.06.045.
[35] Papageorgiou C, Houghton NE, Smith MC. Experimental testing and analysis of inerter devices. J Dyn Syst Meas Control 2009;131:011001https://doi.org/10.1115/1.3023120.
[36] Sun XQ, Chen L, Wang SH, Zhang XL, Yang XF. Performance investigation of vehicle suspension system with nonlinear ball-screw inerter. Int J Automot Technol 2016;17:399–408. https://doi.org/10.1007/s12239−016−0041−x.
[37] Brzeski P, Kapitaniak T, Perlikowski P. Novel type of tuned mass damper with inerter which enables changes of inertance. J Sound Vib 2015;349:56–66. https://doi.org/10.1016/j.jsv.2015.03.035.
[38] Lazarek M, Brzeski P, Perlikowski P. Design and modeling of the CVT for adjustable inerter. J Franklin Inst 2018. https://doi.org/10.1016/j.jfranklin.2018.11.011.
[39] Brzeski P, Lazarek M, Perlikowski P. Experimental study of the novel tuned mass damper with inerter which enables changes of inertance. J Sound Vib 2017;404:47–57. https://doi.org/10.1016/j.jsv.2017.05.034.
[40] Liu X, Jiang JZ, Titurus B, Harrison A. Model identification methodology for fluid-based inerters. Mech Syst Signal Process 2018;106:479–94. https://doi.org/10.1016/j.ymssp.2018.01.018.
[41] Swift SJ, Smith MC, Glover AR, Papageorgiou C, Gartner B, Houghton NE. Design and modelling of a fluid inerter. Int J Control 2013;86:2035–51. https://doi.org/10.1080/00207179.2013.842263.
[42] Ikago K, Saito K, Inoue N. Seismic control of single-degree-of-freedom structure using tuned viscous mass damper. Earthq Eng Struct Dyn 2012;41:453–74. https://doi.org/10.1002/eqe.1138.
[43] Chen MZQ, Hu Y, Huang L, Chen G. Influence of inerter on natural frequencies of vibration systems. J Sound Vib 2014;333:1874–87. https://doi.org/10.1016/j.jsv.2013.11.025.
[44] Basili M, De Angelis M, Pietrosanti D. Modal analysis and dynamic response of a two adjacent single degree of freedom systems linked by spring-dashpot-inerter elements. Eng Struct 2018;174:736–52. https://doi.org/10.1016/j.engstruct.2018.07.048.
[45] Basili M, De Angelis M, Pietrosanti D. Defective two adjacent single degree of freedom systems linked by spring-dashpot-inerter for vibration control. Eng Struct 2019;188:480–92. https://doi.org/10.1016/j.engstruct.2019.03.030.
[46] Marian L, Giaralis A. Optimal design of a novel tuned mass-damper-inerter (TMDI) passive vibration control configuration for stochastically support-excited structural systems. Probabilist Eng Mech 2015;38:156–64. https://doi.org/10.1016/j.probengmech.2014.03.007.
[47] Javidialesaadi A, Wierschem NE. Three-element vibration absorber – inerter for passive control of single-degree-of- freedom structures. J Vib Acoust 2018;140:1–11. https://doi.org/10.1115/1.4040045.
[48] Hu Y, Chen MZQ, Shu Z, Huang L. Analysis and optimisation for inerter-based isolators via fixed-point theory and algebraic solution. J Sound Vib 2015;346:17–36. https://doi.org/10.1016/j.jsv.2015.02.041.
[49] Hu Y, Chen MZQ. Performance evaluation for inerter-based dynamic vibration absorbers. Int J Mech Sci 2015;99:297–307. https://doi.org/10.1016/j.ijmecsci.2015.06.003.
[50] Jin X, Chen MZQ, Huang Z. Minimization of the beam response using inerter-based passive vibration control configurations. Int J Mech Sci 2016;119:1–29. https://doi.org/10.1016/j.ijmecsci.2016.10.007.
[51] Lazar IF, Neild SA, Wagg DJ. Vibration suppression of cables using tuned inerter dampers. Eng Struct 2016;122:62–71. https://doi.org/10.1016/j.engstruct.2016.04.017.
[52] Sun L, Hong D, Chen L. Cables interconnected with tuned inerter damper for vibration mitigation. Eng Struct 2017;151:57–67. https://doi.org/10.1016/j.engstruct.2017.08.009.
[53] Shi X, Zhu S. Dynamic characteristics of stay cables with inerter dampers. J Sound Vib 2018;423:287–305. https://doi.org/10.1016/j.jsv.2018.02.042.
[54] Zhang R, Zhao Z, Pan C. Influence of mechanical layout of inerter systems on seismic mitigation of storage tanks. Soil Dyn Earthq Eng 2018;114:639–49. https://doi.org/10.1016/j.soildyn.2018.07.036.
[55] Zhang R, Zhao Z, Dai K. Seismic response mitigation of a wind turbine tower using a tuned parallel inerter mass system. Eng Struct 2019;180:29–39. https://doi.org/10.1016/j.engstruct.2018.11.020.
[56] Hu Y, Wang J, Chen MZQ, Li Z, Sun Y. Load mitigation for a barge-type floating offshore wind turbine via inerter-based passive structural control. Eng Struct 2018;177:198–209. https://doi.org/10.1016/j.engstruct.2018.09.063.
[57] Ma R, Bi K, Hao H. Mitigation of heave response of semi-submersible platform (SSP) using tuned heave plate inerter (THPI). Eng Struct 2018;177:357–73. https://doi.org/10.1016/j.engstruct.2018.09.085.
[58] Chen Q, Zhao Z, Zhang R, Pan C. Impact of soil–structure interaction on structures with inerter system. J Sound Vib 2018;433:1–15. https://doi.org/10.1016/j.jsv.2018.07.008.
[59] Pan C, Zhang R, Luo H, Li C, Shen H. Demand-based optimal design of oscillator with parallel-layout viscous inerter damper. Struct Control Heal Monit 2018;25:1–15. https://doi.org/10.1002/stc.2051.
[60] Garrido H, Curadelli O, Ambrosini D. Improvement of tuned mass damper by using rotational inertia through tuned viscous mass damper. Eng Struct 2013;56:2149–53. https://doi.org/10.1016/j.engstruct.2013.08.044.
[61] Javidialesaadi A, Wierschem N. Extending the fixed-points technique for optimum design of rotational inertial tuned mass dampers. Conf. Proc. Soc. Exp. Mech. Ser. vol. 2. 2017. p. 10–3.
[62] Javidialesaadi A, Wierschem NE. Optimal design of rotational inertial double tuned mass dampers under random excitation. Eng Struct 2018;165:412–21. https://doi.org/10.1016/j.engstruct.2018.03.033.
[63] Gongyo Pan, Masashi Y. Robust design method of multi dynamic vibration absorber. Trans Jpn Soc Mech Eng Ser C 2005;71:3430–6. https://doi.org/10.1299/kikaic.71.3430.
[64] Yasuda M, Pan G. Optimization of two-series-mass dynamic vibration absorber and its vibration control performance. Trans Jpn Soc Mech Eng Ser C 2003;69:3175–82. https://doi.org/10.1299/kikaic.69.3175.
[65] Ma W, Yang Y, Yu J. General routine of suppressing single vibration mode by multi-DOF tuned mass damper: application of three-DOF. Mech Syst Signal Process 2019;121:77–96. https://doi.org/10.1016/j.ymssp.2018.11.010.
[66] Asami T. Optimal design of double-mass dynamic vibration absorbers arranged in series or in parallel. J Vib Acoust 2016;139:011015. https://doi.org/10.1115/1.4034776.
[67] Asami T, Mizukawa Y, Ise T. Optimal design of double-mass dynamic vibration absorbers minimizing the mobility transfer function. J Vib Acoust 2018;140:061012. https://doi.org/10.1115/1.4040229.
[68] Jang SJ, Brennan MJ, Rustighi E, Jung HJ. A simple method for choosing the parameters of a two degree-of-freedom tuned vibration absorber. J Sound Vib 2012;331:4658–67. https://doi.org/10.1016/j.jsv.2012.05.020.
[69] Barredo E, Colín J, Penagos VM, Abúndez A, Vela LG, Meza V, et al. Closed-form solutions for the optimal design of inerter-based dynamic vibration absorbers. Int J Mech Sci 2018;144C:41–53. https://doi.org/10.1016/j.ijmecsci.2018.05.025.
[70] Asami T. Optimal design of double-mass dynamic vibration absorbers arranged in series or in parallel. J Vib Acoust 2016;139:1–16. https://doi.org/10.1115/1.4034776.
[71] Marian L, Giaralis A. Optimal design of a novel tuned mass-damper-inerter (TMDI) passive vibration control configuration for stochastically support-excited structural systems. Probabilist Eng Mech 2014;38:156–64. https://doi.org/10.1016/j.probengmech.2014.03.007.
[72] Crandall S, Mark W. Transmission of random vibration. Random Vib Mech Syst 1963:55–102.
[73] Kreyszig E. Residue integration method. Adv. Eng. Math. 10th ed.; 2011. p. 719–32.
[74] Forst W, Hoffmann D. Global optimization. Optim. Theory Pract. New York, NY: Springer New York; 2010 [chapter 8].
[75] Nishihara O, Asami T. Closed-form solutions to the exact optimizations of dynamic vibration absorbers (minimizations of the maximum amplitude magnification factors). J Vib Acoust 2002;124:576. https://doi.org/10.1115/1.1500335.